

MNRAS, Submitted February 10, 1995; Accepted June 16, 1995

X-ray Timing and Spectral Behavior of the Rapid Burster

Robert E. Rutledge¹, Lori M. Lubin², Walter H.G. Lewin¹,
Brian Vaughan³, Jan van Paradijs^{3,4}, and Michiel van der Klis³

¹ Massachusetts Institute of Technology, Room 37-627, Cambridge, MA 02139, U.S.A.

² Princeton University Observatory, Peyton Hall, Princeton, NJ 08544-1001, U.S.A.

³ Astronomical Institute “Anton Pannekoek”, University of Amsterdam, Center for High Energy Astrophysics, Kruislaan 403, 1098 SJ Amsterdam, The Netherlands

⁴ Physics Department, University of Alabama in Huntsville, Huntsville AL 35899

Abstract

We present an X-ray fast-timing and spectral analysis of the type II bursts and the persistent emission (PE) of the Rapid Burster observed with the *EXOSAT* Medium-Energy Instrument. The Hardness-Intensity and Color-Color Diagrams of the Rapid Burster are somewhat different from those of the majority of other low-mass X-ray binaries, which fall into two distinct groups, “atoll” and “Z” sources. The strength and frequencies of quasi-periodic oscillations (QPO) in the bursts and the PE, as well as a strong anti-correlation between QPO frequency and burst peak flux, also distinguish the Rapid Burster from atoll and Z sources.

The presence, frequency, and strength of QPO in type II bursts are all correlated in some manner to the spectral hardness, as are the strength of QPO and the very low-frequency noise (VLFN) component in the persistent emission.

1. Introduction

Discovered in 1976 by Lewin et al. (1976), the Rapid Burster (MXB 1730-335, or “RB” herein) is located in the highly reddened globular cluster Liller I (Liller 1977) at a distance of ~ 10 kpc (Kleinmann, Kleinmann & Wright 1976). The Rapid Burster is the only low-mass X-ray binary (LMXB) which produces two types of X-ray bursts (Hoffman, Marshall & Lewin 1978). Type I bursts, which are observed from ~ 40 other LMXB, are due to thermonuclear flashes on the surface of an accreting neutron star (NS). Type II bursts, which are unique to the Rapid Burster, are the result of accretion instabilities (gravitational potential energy). The behavior of the type II bursts can be described as that of a relaxation oscillator; the integrated flux (E) in a burst is roughly proportional to the time interval (Δt) to the following burst (Lewin et al. 1976; Lewin 1977; White 1978; Marshall et al. 1979; Inoue et al. 1980). For a detailed review, see Lewin, Van Paradijs & Taam (1993).

The Rapid Burster exhibits at least two type II burst modes: mode I is characterized by bursts with a bimodal duration distribution, while mode II has a unimodal duration distribution (Marshall et al. 1979). At times type II bursts are observed with strong persistent X-ray emission (PE) after long (> 30 sec) type II bursts. This persistent emission emerges gradually after a long type II burst and disappears before the occurrence of the next type II burst; this disappearance just before and after bursts is referred to as the “dips” in the persistent emission (Marshall et al. 1979; Van Paradijs, Cominsky, & Lewin 1979; Stella et al. 1988a). These dips are not likely to be due to an obscuration of the source (Lubin et al. 1993). The persistent emission between bursts also exhibits distinct features such as strong 40 mHz oscillations, small bumps and glitches, and a characteristic “hump” in its profile (Lubin et al. 1992b, 1993).

Lubin et al. (1992a) reported that the relation between burst peak luminosity and peak black-body temperature depends only on the characteristic mode of recurrence of

the type II bursts, independent of their duration (from ~ 2 to ~ 680 sec). For bursts during the mode II (single distribution of durations) there exists a correlation between peak luminosity and black-body temperature (Kunieda et al. 1984; Kawai et al. 1990; Tan et al. 1991) while bursts in mode I (bimodal distribution of durations) have an approximately constant temperature (Lubin et al. 1992a). For type II bursts during mode II, Kawai et al. (1990) and Tan et al. (1991) found an anti-correlation between blackbody temperature and instantaneous burst flux.

Many type II bursts with durations in excess of ~ 9 sec show quasi-periodic oscillations (QPO) in the $\sim 2 - 7$ Hz range (Tawara et al. 1982; Stella et al. 1988a; Dotani et al. 1990; Lubin et al. 1991). QPO have also been seen in bursts with durations as short as ~ 3 sec (Rutledge et al. 1995). The average QPO centroid frequency during a burst is strongly anti-correlated with the average burst peak flux (except perhaps at low peak fluxes where they may be correlated; see Lubin et al. 1991). QPO with frequencies of 2-5 Hz have also been discovered in the persistent emission observed after type II bursts with durations between ~ 60 and 120 sec; in several cases the QPO evolved from ~ 4 Hz just after the burst to ~ 2 Hz. The frequency of the QPO was positively correlated with the spectral hardness of the persistent emission, such that the spectrum softened as the QPO frequency decreased. Occasionally, frequencies of $\sim 0.4 - 1.0$ Hz were also detected (Stella et al. 1988a). QPO of frequencies ~ 0.04 Hz have also been found to sometimes occur at the onset of the persistent emission just after the post-burst dip, correlated with the occurrence of a spectrally hard “hump” and with the appearance of 4 Hz QPO (Lubin et al. 1992b).

Dotani et al. (1990), using the X-ray detector LAC on *Ginga* (Turner et al. 1989), observed QPO from the type II bursts of the Rapid Burster, and was able to pick out individual oscillations in the QPO, and observed the slow change of the frequency of the QPO.

All of the neutron-star low-mass X-ray binaries are a member of one of two distinct groups called Z sources and atoll sources (Hasinger and Van der Klis 1989 – hereafter HK89). Sources in both groups show a strong correlation between their X-ray spectral and fast-variability properties. In this paper, we present a study of the X-ray timing and the spectral behavior of type II bursts and persistent emission of the Rapid Burster in light of the source classification of other LMXB.

A previous attempt to describe the fast-timing behavior of type II bursts from the Rapid Burster in terms of the Z/atoll paradigm has been made by Dotani et al. (1990). They found that the timing behavior (*i.e.* QPO and noise) in the type II bursts are most similar to behavior in the Normal Branch (NB) of Z sources (HK89); however, if the NB QPO are explained by a near-Eddington process (see Van der Klis 1994 and references therein), then the large range of burst peak fluxes in which the 2-5 Hz QPO are observed may argue against a common origin for RB burst QPO and NB oscillations.

In Section 2, we describe the data used in the present analyses. In Section 3, we analyze the spectral and timing behavior of the persistent emission. In Section 4, we perform a similar analysis on the bursts. In Section 5, we take a closer look at the 1985 observations to compare the bursts and persistent emission behaviors with each other and with the observed behaviors in other LMXB. In Section 6, we discuss the results of these analyses in

the context of the Z/Atoll paradigm and present our conclusions.

Throughout this paper, when we refer to “burst numbers” for bursts observed during the August 1985 observations, we use the sequential numbering of these bursts by Stella et al. (1988a) and Lubin et al. (1992b). The term “bursts” refers only to the type II bursts, unless it is explicitly stated that we refer to type I bursts. Also, all power density spectra shown are normalized according to Leahy et al. (1983).

2. The Observations

The Rapid Burster was observed with the Medium Energy (ME) Argon detector array (Turner, Smith & Zimmerman 1981) of *EXOSAT* on eight occasions. We have analyzed six of these observations, excluding those two (1983 August 7 and 1983 August 26) which were made with 4U/MXB 1728-34 in the field-of-view (FOV). Data were selected which had high time resolution ($\lesssim 150$ ms) with at least 4 energy channels, and which were obtained when 1728-34 was completely excluded from the FOV. The selected data are indicated in Table 1. We chose to include the 1984 July 17 observation for completeness in the spectral part of this study, despite the fact that Lubin et al. (1991) found no evidence for QPO in the bursts in this observation. Because there were no QPO in these bursts, we did not analyze these data for the burst timing properties.

In the following, we briefly summarize some basic characteristics of the RB during these individual *EXOSAT* observations, and give references to previous work based on them.

- *1983 August 15* This observation has been described by Barr et al. (1987). During this observation, the Rapid Burster was observed to give off strong persistent emission and type I bursts, but no type II bursts were observed. For the first three and last five hours of this 24 hour observation, the ME was pointed directly at the Rapid Burster, placing 4U/MXB 1728-34 at a collimator efficiency of 21%. From 00:57 to 9:58, the Rapid Burster was observed with a collimator efficiency of 28%, while 4U/MXB 1728-34 was excluded from the FOV. During this period, the Rapid Burster was observed with one-half of the ME array, while the other half observed the (off-source) background.
- *1984 July 17* One half the detector array contained only the Rapid Burster, the other one only 4U/MXB 1728-34, at transmission efficiencies of $\sim 35\%$ and $\sim 40\%$, respectively. Thus, the overall transmission efficiency (in reference to the full array) was $\sim 17.5\%$ and $\sim 20\%$ for the Rapid Burster and for 1728-34, respectively. Background (off-source) data were taken from UT July 18, 06:27-07:34. A total of 243 type II bursts were observed in this observation. No persistent emission was detected, and the type II bursting activity is characterized by mode II. Results from this observation have been presented by Lubin et al. (1991) and Tan et al. (1991).

- *1985 August 28-29* During the first 2.3 hours (with the exception of a 15 min period; see Stella et al. 1988a) the transmission efficiencies (referenced to the full detector array) for the Rapid Burster and the nearby source 4U/MXB 1728-34 were $\sim 41\%$ and $\sim 100\%$, respectively. After UT 17:45 1728-34 was excluded from the FOV and the transmission efficiency for the Rapid Burster was 48%. The persistent emission was highly variable. Strong $\sim 2 - 4$ Hz and 0.04 Hz QPO (and occasionally $\sim 0.4 - 1.0$ Hz QPO) were observed in the persistent emission as well as $\sim 2 - 5$ Hz QPO in the type II bursts. Background (off-source) data were taken from UT August 28, 14:54 - 15:23. During the entire observation, one of the eight detectors was turned off. Between UT August 29, 1:00 and 9:35 (the end of the observation), one of the seven operating detectors malfunctioned producing an artificial flaring phenomenon. This was identified by “flaring” types of events in only one detector in the housekeeping data, which were not seen in any of the other active detectors. Some data during this period could not be fully analyzed. A total of 40 type II bursts were observed during the observation. Although the bursts were all very long (90–680 sec), the burst activity is best described as mode I. Results from this observation have been presented by Stella et al. (1988a,b), Tan et al. (1991), and Lubin et al. (1992b, 1993).
- *1985 August 30-31* Between UT August 30, 18:28 and August 31, 00:10 and between UT August 31, 02:24 and 07:33, both half arrays were pointing in the same direction, and the Rapid Burster was observed with a transmission efficiency (referenced to the full array) of $\sim 46\%$; 4U/MXB 1728-34 was not in the FOV. Background (off-source) data were taken from UT August 30, 17:08 - 18:28 and from UT August 31, 07:34 - 07:45. In addition, one half array was pointed at the background (off-source) between UT August 31, 00:10 and 01:10; the other half was off-source between UT August 31, 01:10 and 02:15. The frequencies of QPO observed during this observation are the same as observed during 1985 August 28-29, except that the frequencies of QPO in the bursts were in the range 2-3 Hz. A total of 55 type II bursts were observed during this observation. Although the bursts were all very long (40–200 sec), the burst activity is best described as mode I. (For details on these observations, see Stella et al. 1988a, b; Tan et al. 1991; Lubin et al. 1992b, 1993.) During the entire observation, one of the eight detectors was turned off (the same one as during the Aug 28-29 observations). Results from this observation have been presented by Stella et al. (1988a,b), Tan et al. (1991), and Lubin et al. (1992b, 1993).
- *1985 September 10 and 13* The Rapid Burster, when observed, was in the FOV of both half arrays with a transmission efficiency (referenced to the full array) of $\sim 43\%$; 1728-34 was outside the FOV. 371 type II bursts were observed on September 10, 1985 and 170 on September 13 1985. QPO with centroid frequencies of 5-7 Hz were observed in bursts of duration 9-30 seconds. There was no persistent emission detected in these observations. The type II bursting activity was characteristic of mode II. Background was taken during the inter-burst periods. Results from these observations have been presented by Tan et al. (1991) and Lubin et al. (1991).

3. The Persistent Emission

Persistent emission (PE) was observed between type II bursts from the Rapid Burster with *EXOSAT* during the observations on 1985 August 28-29, and 1985 August 30-31. On Aug 15, 1983 persistent emission was detected, but no type II bursts were observed. Persistent emission was not detected during the Sept 10 & 13 1985 observations, nor during the July 17 1984 observations.

3.1. PE Spectral Analysis

3.1.1. PE Spectral Analysis: 1983 August 15

Figs. 1a & b shows Hardness-Intensity Diagrams (HIDs) and Fig. 1c shows the Color-Color Diagram (CCD) of the persistent emission observed during the 1983 August 15 observation for a “soft” color (5.7 - 9.3 keV/2.0 - 5.7 keV) and a “hard” color (9.3 - 17.0 keV/5.7 - 9.3 keV). The 1σ error bars are indicated on each data point. Each point represents an integration time of 600 seconds. Type I bursts were not included in the HIDs, nor in the CCD. All counting rates were corrected for aspect and normalized to the full array area. As the count rates were low, it was not necessary to correct them for dead time, which we estimate is $\sim 1\%$. While the persistent emission count rate varies by $\sim 25\%$, the hard color and the soft color vary $\sim 15\%$; (Figs. 1a & b).

The CCD (Fig. 1c) does not indicate any significant correlation between either the hard or soft colors with the X-ray intensity; the hard and soft colors are themselves correlated, however this is not surprising as they share an energy band. Using a Spearman rank-order correlation test, we find probabilities of 34%, 92%, and 99.9% for the data shown in Fig. 1a, b, and c, respectively. The existence of the correlation between the hard and soft colors indicates measurable spectral evolution in the persistent emission of this data. The *general* trend of this evolution is a decreasing soft color and an increasing hard color (referring to Fig. 1c, the motion in the CCD with increasing time is from the lower right corner towards the upper left corner).

Because the 15 August 1983 observation was taken with different energy channel boundaries than those in the other observations, the energy ranges are very different from those of other observations. This, unfortunately, complicates a comparison of CCDs and HIDs between this and the other observations.

3.1.2. PE Spectral Analysis: 1985 August 28-29 & 30-31

During the course of the 30-31 August 1985 observation, the On Board Computer (OBC) mode was changed, resulting in different selections of energy channel ranges. For a period while the OBC mode HER7 (hereafter, “I7”; Andrews & Parmar 1985) was active, the selected energy ranges overlapped – but did not exactly match – the energy ranges for the remainder of the observation. We overcame this by correlating contemporaneous data from earlier in the observation when both OBC modes I7 and HER5 (hereafter, “E5”; which had sufficient energy resolution) were active. Comparing the background-subtracted count rates in the E5 energy ranges with the corresponding I7 energy ranges (integrated over 20 sec), we were able to derive linear relations between the E5 and I7 count rates.

The linear fits to the data in the three energy channels used in this analysis were quite good, with little systematic deviation, introducing an acceptably small systematic uncertainty ($\lesssim 7\%$). In Table 2, we show the parameters for linear conversion of counts in the first three energy ranges of the form $(\text{countsE5}) = m \times (\text{countsI7}) + b$.

Figure 2 shows the HIDs and CCD of the persistent emission as observed during the observations 1985 August 28-29 and 30-31 for a soft color (3 - 5 keV/1 - 3 keV) and a hard color (5 - 10 keV/3 - 5 keV). Each point represents an integration of 100 seconds. A sample error bar is included in each panel. All counting rates (1-20 keV) have been normalized to the full array area and corrected for background, aspect, and dead time (Stella & Andrews 1985). While the count rate changes substantially (up to a factor of 2; panels a, b, d & e), the hard and soft colors also vary, although not systematically. Using a Spearman rank-order correlation test, probabilities of spurious correlation of the magnitude observed in these panels range between 95-98%. Fig. 2c shows that the hard and soft colors are uncorrelated, with a Spearman rank-order correlation test probability of 92%; however, the hard and soft colors were correlated on Aug 30-31 (Fig. 2f), with a probability of being spuriously generated of $\sim 4 \times 10^{-10}$. This cannot be due to a systematic shift of the corrected I7 data; we analyzed the E5 data separately from the corrected I7 data, and found that they separately have probabilities of $\sim 2 \times 10^{-4}$ and $\sim 1 \times 10^{-7}$ of being produced spuriously. Thus, there is a correlation in colors observed in the Aug 30-31 data which is not observed in the Aug 28-29 data.

To illustrate the distribution of intensity and hardness in the persistent emission, Figure 3 shows the distribution of the average intensities (1 - 20 keV) and the hard and soft colors of the persistent emission intervals (100 sec integrations) for both observations. The spectrum of the persistent emission, observed during the August 30-31 observation, is *harder* in the hard color and *softer* in the soft color than that observed during August 28-29 (Figure 3, bottom panel). This indicates that the 3-5 keV range decreased in total fluence relative to the 5-10 keV and 1-3 keV range between these two observations, even while the count-rates remained roughly constant. The distributions of the hard ratios on the different days are considerably distinct, whereas that of the soft ratio is less so, and the intensity even less so. This indicates that, even while the countrates may remain constant, the relative spectrum at high energy (> 5 keV) varies with greater magnitude than at low energies (< 5 keV).

The weighted averages of the PE hard color (5 - 10 keV)/(3 - 5 keV) and the soft color (3 - 5 keV)/(1 - 3 keV) of the August 28-29 observations are 0.765 and 2.052 and of

the August 30-31 observation are 0.824 and 2.017, respectively. The formal errors on these values are <1%.

3.2. PE Timing Analysis

We have examined several timing features of the Rapid Burster persistent emission using Power Density Spectra (PDS). These are (a) the VLFN component, (b) ~ 0.04 Hz QPO, and (c) QPO for centroid frequencies in the range 2-6 Hz. High Frequency Noise (HFN) is discussed in the following section. We parameterize these features by fitting them, using a least- χ^2 method, with the models:

$$P_{\text{Lor}}(\nu, \nu_c) = \frac{A_{\text{Lor}}}{\pi} \frac{(\Gamma/2)^2}{(\nu - \nu_c)^2 + (\Gamma/2)^2} \quad (1)$$

$$P_{\text{pl}}(\nu) = A_{\text{pl}} \nu^{-\alpha} \quad (2)$$

$$P_{\text{const}} = A_0 \quad (3)$$

$$P(\nu) = P_{\text{const}} + P_{\text{pl}}(\nu) + \sum_{i=1}^N P_{\text{Lor}}(\nu, \nu_i) \quad (4)$$

where ν is a frequency, A_{lor} is the area under a Lorentzian peak integrated $-\infty < \nu < \infty$, ν_c is the centroid frequency, Γ is the full-width at half-maximum (FWHM) of the Lorentzian, N is the number of fit QPO peaks (usually 1–3) and A_{pl} and A_0 are constants. P_{lor} is used for modelling the QPO, P_{pl} is used for modelling the VLFN, and P_{const} is used to model the Poisson level.

3.2.1. PE Timing Analysis: 1983 August 15

The variability of the persistent emission in the 1983 Aug 15 observation has been investigated by Barr et al. (1987). For QPO with a FWHM of $\sim 15\%$, they found that “At a 90% confidence level the upper limits to the RMS amplitude of the QPO ranged from $\sim 9\%$ to $\sim 12\%$ (depending on frequency)” for frequencies in the range 2-5 Hz. A more general search for “coherent and quasi-periodic oscillations in the frequency range 0.06 to 64 Hz” was performed, the results of which were that “The source power density spectrum did not reveal any significant excess variability above Poisson noise.”

We have searched for excess Very Low Frequency Noise (VLFN) in this data set. We produced 12 FFTs of frequency range 0.00065-5.6 Hz, using data in the 5.9-17 keV energy range, being careful to avoid telemetry breaks and type I bursts. As there was little spectral evolution in the dataset (<15%) we did not sort the FFTs by hardness. The FFTs were

summed into a single PDS. In Fig. 4, we show the PDS, rebinned logarithmically (panel a) and linearly (panel b). The evidence for VLFN (modelled as a power-law plus a constant Poisson level) is marginal, with a 2σ upper limit in the frequency range 0.00065-1.0 Hz of 2.0%, and requiring a very steep power-law slope ($\alpha=3.3$). We also fit a Lorentzian plus a constant to the PDS (rebinned linearly to 112 bins) to search for QPO with FWHM $\sim 25\%$ at $\nu=2, 3, 4$, and 5 Hz. We find no evidence for QPO; 2σ upper limits on the %rms were in the range 8 - 10%, consistent with the upper-limits found on narrower QPO by Barr et al. (1987). Visual inspection of the PDS (Fig. 4b) shows no evidence for QPO-like behavior at any frequency.

3.2.2. PE Timing Analysis: 1985 August 28-29 & 30-31

To investigate the fast-timing properties of the persistent emission, we performed a Fourier analysis using the high time resolution I5 and I7 data in the energy range 1 - 20 keV (see Section 2.).

Successive fast Fourier transforms (FFTs) were made of each persistent emission interval, beginning after the dip (see Introduction) following each burst, when the 1-sec average count rate became 90% of the following PE mean count rate. Each FFT was 128 sec long with a Nyquist frequency of 16 Hz. FFTs were made sequentially in each interval until there was no longer enough data for an FFT before the dip which precedes the next burst. The resulting PDS (a total of 454) were sorted according to their average hard color (5 - 10 keV/3 - 5 keV). The PDS averaged into six hard color intervals are shown in Figure 5 with their least- χ^2 models, from which the strength of the spectral features (VLFN & QPO) were found (see below, and Tables 3 & 4). The PDS have been logarithmically rebinned to better show the VLFN component; the dead time affected Poisson level (fit as a constant) has been subtracted. The frequency bins where the power was consistent with (less than 1σ greater than) zero are plotted with 2σ upper limits (indicated by solid symbols and an arrow pointing downwards); otherwise, the power in each bin is shown with a 1σ error bar. The number of FFTs and the range of the hard color of each averaged PDS are indicated in the upper right of each panel. The best fit model often lies below the plotted points, as the model takes into account the data which are consistent with zero power (here, plotted as 2σ upper limits).

The PDS of the persistent emission exhibit several distinct features which vary with hard color. As previously shown in Figure 9 of Stella et al. (1988a), the frequency of the QPO increases from ~ 2 Hz to ~ 4 Hz with increasing hard color (Figures 5c,d,e,f). For the 2-5 Hz QPO in the PE we find, for the three softer color ranges, roughly constant %rms values of ~ 8 -11%. In the fourth hard color range (0.82-0.86), the QPO %rms increased (to 16.5%) and the peak becomes much broader (FWHM = 5.0 ± 0.4). To account for multiple peaks in the PDS of the two hardest ranges, we fit two Lorentzians to the data. To determine the total %rms under these double peaks, we summed the total power under both Lorentzians. We find that the %rms is $17.1 \pm 1.9\%$ and $26.2^{+1.7}_{-3.4}\%$ in the two hardest color intervals.

Only the *harder* portions of persistent emission exhibit the ~ 40 mHz oscillations (Figures 5e,f), consistent with the results found by Lubin et al. 1992b. The width of the 0.04 Hz peak is systematically ill-constrained in panel f due to the poor frequency resolution. No ~ 0.04 Hz QPO are detected when the persistent emission is softest. A 2σ upper-limit to QPO in the 0.82-0.86 range is $\leq 2.5\%$ (rms). The %rms increases in the harder PE (>0.86 hard color) confirming the correlation with hard color of 0.04 Hz QPO as first seen in this data by Lubin et al. (1992b). However, we are unable to significantly constrain the %rms (2σ upper limit $\sim 84\%$) in the hardest PE due to poor frequency sampling.

The strength of the VLFN, integrating a power-law fit from 0.0078-1.0 Hz, shows a clear correlation in %rms with hard color, increasing from $<2.9\%$ to 17.5% with increasing hard color. This may be due, in part, to the appearance of several “flare” -type features in the intensity profiles of this observation which have a very hard spectrum; additionally, these may be due to the “humps”, which sometimes appear in the PE just after the dip following the burst, and which are correlated with the appearance of the 0.04 Hz QPO and the presence of a hard spectrum (see Lubin et al. 1992b). It is important to note that VLFN with a steep power law slope ($\alpha \gtrsim 2.0$) is susceptible to low-frequency leakage (see Van der Klis 1989).

To investigate the contribution to the PDS by the “hump” (see Introduction) in the PE, we excluded from the analysis the first 256 seconds of persistent emission following the start of the hump. The resulting PDS are shown in Fig 6, and were produced as described above. The least χ^2 fit parameters are listed in Table 5, and the %rms values of the different features derived from these parameters are listed in Table 6. The fits were largely poor, with very high χ^2 values.

It is clear that the low frequency power is diminished when the hump is excluded, and is therefore probably due to the hump itself (and thus, is not VLFN). The power-law slopes were, in some cases, unmeasurable. The strength of the low frequency power increased with increasing hardness (from ≤ 2.2 to $7.5^{+1.4}_{-1.8}\%$ rms), however dropping in the very hardest range to 3.5 ± 0.6 .

The exclusion of the “hump” has little qualitative or quantitative effect on the dependence of QPO parameters on spectral hardness.

The strength of the QPO with the first 256 sec following bursts excluded (Table 6) is nearly identical as a function of spectral hardness to strength of the QPO when the first 256 sec are included (Table 4). The QPO % rms (0.01-100 Hz) as a function of spectral hardness is largely constant, with a small dip in the middle spectral range and a jump at the hardest spectral range.

High Frequency Noise. Using the available HTR3 (hereafter, “T3”) data, we have searched for High Frequency Noise (HFN) above 10 Hz in the persistent emission. The T3 data has very high time resolution (≤ 4 ms) with no energy resolution (1 channel; $\sim 1 - 22$ keV).

Data were available for 36 persistent emission intervals (i.e. 36 between-burst intervals) during the August 1985 observations. Each interval was divided up into consecutive 128 second stretches, each of which produced a single FFT. The FFTs were averaged together

into a single PDS for each persistent emission interval, and the Poisson level, calculated as described in Van der Klis (1989), was subtracted. The %rms value was determined in two frequency ranges: 10-100 Hz and 20-60 Hz. These were selected because they are the frequency ranges where the HFN is dominant in the Z-sources and where the QPO in the horizontal branch occurs in the Z-sources (HK89). The %rms was measured by summing the Poisson-level subtracted power in the relevant frequency range. Of the 36 PE intervals, one (following burst # 41) had measured HFN in the 10-100 Hz frequency range at a significant level ($18 \pm 3\%$). One PE interval (following burst # 58) had a significant %rms ($16 \pm 3\%$) value in the frequency range 20-60 Hz. The other 35 PE intervals had 2σ upper limits to their HFN in the range of 15%-62%, with most upper-limits below 30%. With all FFTs from all 36 PE intervals averaged into one PDS, the 2σ upper limits to the HFN in the 10-100 Hz range and 20-60 Hz range were 8.0% and 10.0%, respectively.

We also sorted these persistent emission FFTs by their hardness and produced averaged PDS. No hard color range produced a detection of HFN, in either the 10-100 Hz or 20-60 Hz ranges, with 2σ upper limits of 13-22% and 10-17%, respectively.

4. The Type II Bursts

4.1. Spectral Analysis

Figure 7 shows HIDs and CCDs of all five observation periods in which type II bursts were observed from the Rapid Burster (1984 July 17, 1985 August 28-29, 1985 August 30-31, 1985 September 10 & 13). The observation period is indicated at the top of each column. Each data point represents all data from a single burst. For 1984 July 17 and 1985 September 10 & 13 observations, when the bursts were relatively short (“short-burst observations”) data were integrated from the first point which is $>5\sigma$ above background to the first point which is 0.5σ below background. For the “long-burst observations” (1985 August 28-29 & 30-31), data were integrated from the first of two consecutive time bins in which the count rate is greater than 6σ above the pre-burst persistent emission level, and the burst end is defined as the first of two consecutive time bins in which the count rate is within 2σ of the post-burst persistent emission level (excluding the dip). The difference between the burst-start and burst-end definitions is due to the fact that long bursts have many more integrated counts than the short bursts and we can afford greater precision in delimiting their start and end; short bursts, however, must be delimited with the requirement of maximizing the integrated signal/noise.

Each panel in Fig 7 contains an average 1σ error-bar, located at the same coordinate along the same row. These error bars are not located at actual data points.

Figure 7 shows the burst peak count rate vs. burst hard color (5-10 keV/3-5 keV; panels a-e) and vs. burst soft color (3-5 keV/1-3 keV; panels f-j). The peak count rate is the highest ~ 1 sec time-bin count rate during the burst, and has been corrected for background (see Section 2.), dead time (see Stella & Andrews 1985; eq. 3.10 of Van der Klis 1989), aspect, and renormalized to the full detector array area. Background was subtracted from the channel count rates prior to calculating the colors. Peak flux was selected as a discriminator as the spectral properties of the bursts are a function of the burst peak flux (*i.e.* brighter bursts are harder, and have lower QPO centroid frequencies than fainter bursts; see Introduction).

Figs. 7k-o show the CCDs of soft color (3-5 keV/1-3 keV) vs. hard color (5-10 keV/3-5 keV). Immediately, one’s eye is caught by the extended branches observed during the long-burst observations. This is most evident in the CCD (Figs. 7l,m), but it is also evident in the soft color HIDs (Figs. 7g,h) and the hard color HID (Fig. 7b; the hard-color HID in Fig. 7c shows more an amorphous and extended “cloud” than a branch).

These well-defined branches stand in contrast to the “clouds” observed during the other three observation periods (1984 July 17, 1985 Sept 10, and 1985 Sept 13; Figures 7a,d,e,f,i,j,k,n,o). The peak count rates and the dynamic range of the peak count rates during the long-burst observations are larger (by a factor of ~ 1.5 in peak count rate, and ~ 1.5 -2.2 in dynamic range) than those observed during the short-burst observations.

The previously reported correlation between burst peak counting rate and spectral hardness (or equivalently blackbody temperature) for long (> 30 sec) type II bursts (Kunieda et al. 1984; Tan et al. 1991; Lubin et al. 1992a) is clearly evident in the HIDs of both observations.

The bursts observed during the August 28-29 observation have a larger dynamical range in hardness than those observed on August 30-31. Bursts with relatively low average peak intensities ($\sim 1200 - 1400$ counts/s; $1 \text{ count/s} \simeq 1.6 \times 10^{-11} \text{ ergs cm}^{-2} \text{ s}^{-1}$; see Tan et al. 1991) and therefore with softer spectra were only observed during the August 28-29 observation. The weighted averages of the hard color (5 - 10 keV)/(3 - 5 keV) and the soft color (3 - 5 keV)/(1 - 3 keV) of the August 28-29 observations are 0.94 ± 0.01 and 2.93 ± 0.03 and of the August 30-31 observation are 0.99 ± 0.01 and 2.98 ± 0.01 , respectively (see Table 7).

Table 7 gives the weighted mean burst hard (5-10 keV/3-5 keV) and soft (3-5 keV/1-3 keV) colors for these five observations. The spectral state of the 1984 July 17 cannot be directly compared to that of the 1985 observations, as changes in the EXOSAT ME calibration can account to up to a 10% shift in the hardness ratios in these channels (see below). Comparing the 1985 observations, however, the hard ratio is lowest during the 1985 Sept 13 observation (0.892 ± 0.003).

By averaging the short-burst colors and intensities some structure is revealed in the “clouds” of Fig. 7. The composite HIDs and CCDs of Fig. 8 illustrate this. The observation period is indicated by the legend in the figure. For the short-burst observation periods, we plot the average hard and soft colors of bursts with 1-20 keV peak count rates within consecutive peak count rate ranges; these ranges are indicated as error bars in peak count rate. The error bars on hardness for July 1984 and September 1985 are the 1σ uncertainties

in the mean hardness. Each point from the long-burst observations represents data from a single burst ($\gtrsim 40$ s). The average 1σ uncertainty is indicated as an error bar on a single point for each of these two observation periods. All count rates have been corrected for dead time, aspect, and normalized to the full EXOSAT ME array area.

In both the HIDs and the CCD in Figure 8, the July 1984 bursts are separated from the other bursts, occupying a completely different area on the HIDs and CCD. We investigated if this separation could be due to the change in the EXOSAT ME energy response. We assumed a detector energy response which was Gaussian, with a centroid energy, detector efficiency, and FWHM as given by the relevant EXOSAT calibration file. We assumed a source thermal spectrum with a galactic absorption component with $N_h = 1.5 \times 10^{22} \text{ cm}^{-2}$ (see, for instance, Lubin et al. 1992a). We did this for three separate temperatures, $kT = 1.5, 1.85, 2.2 \text{ keV}$. We find a systematic shift in the soft ratio of $<1\%$ and a systematic shift in the hard ratio of $\sim 10\%$ between the 1984 and 1985 calibrations. The shift in the hard ratio due to the calibration shift of EXOSAT can completely account for the separation in the hard ratio between 1984 and 1985 observations seen in Fig 8b. However, it cannot account for the shift in the soft ratio in Fig. 8c.

4.2. Timing Analysis

In this section, we present the results of a timing analysis of bursts in the August 1985 and September 1985 observations. We did not analyze the July 1984 observation for timing properties, as a previous study (Lubin et al. 1991) observed no QPO in these bursts. To attempt to deconvolve the LFN from the burst profile is not useful, given that the burst durations were short (largely 3-12 seconds) and most of the broad-band structure is due to the burst profile (see Tan et al. 1991).

4.2.1. Burst Timing Analysis: 1985 August 28-29 & 30-31

To investigate the fast-timing properties of the bursts we performed a Fourier analysis using the high time-resolution I5 (HER5 data-type, but with no energy resolution), I7, and T3 data in the energy range 1 - 20 keV.

Power Density Spectra. Successive FFTs were made of each burst peak between the peak start and end. To avoid the sharp rise of the burst, the peak start was somewhat arbitrarily defined as the first in three consecutive 1-sec time bins where the average count rates in the following two bins are no more than 2σ greater than that in the first bin. The peak end was defined as the first bin in the first series of two bins (1 sec integration each) in which the count rates were both more than 2σ below the average counting rate up to that point; the characteristic ringing and humps (Tan et al. 1991) are thus not analyzed.

The shortest burst peak (defined in this way) was 18 seconds. Each FFT was 16 sec long (with a Nyquist frequency of 16 Hz); therefore, each burst consisted of one or more FFTs depending on the burst duration. The resulting FFTs (a total of 455 for both observations) were sorted according to the hard color (5 - 10 keV/3 - 5 keV) of the PDS interval (not according to the hard color of the entire burst). Figure 9 shows the average PDS of these six hard color intervals. The number of FFTs and the hard color range of each averaged PDS are indicated in the upper left of each panel. The dead time affected Poisson level has not been subtracted. The solid line in each panel is the least- χ^2 best fit model, found as described below (see Tables 8 & 9).

QPO Frequencies. The dominant feature in several of the averaged power density spectra is a QPO peak. The QPO frequency decreases from ~ 5 Hz for the softest bursts to ~ 2 Hz for the hardest bursts. For PDS of the softer (0.74-0.98) periods, the mean QPO frequency is measured to be 4.4 - 4.9 Hz, while for the harder periods (0.98-1.12), the QPO frequency is measured to be 2.0 - 2.5 Hz (see Table 8). QPO at frequencies 2-5 Hz manifest themselves in the hardness range 0.92-0.98 as a broad peak ($\Gamma = 1.7$ Hz). Though the average PDS of the bursts seem to show QPO frequencies of ~ 2 and ~ 5 Hz (Figure 9), the centroid frequencies in individual bursts actually extend almost uniformly from ~ 3.5 - 5 Hz and from ~ 2 - 2.5 Hz (see Fig. 3 of Stella et al. 1988a). The *general* anti-correlation between QPO frequency and burst hardness is expected as the frequency of QPO in long (> 30 sec) bursts is anti-correlated with the burst peak intensity (Stella et al. 1988a), and the burst peak intensity is correlated with hardness (Kunieda et al. 1984; Tan et al. 1991; Lubin et al. 1992a; Figure 12).

Fractional rms Variations. Table 9 shows the %rms variation (dead time and background corrected) in the VLFN component and the QPO($\nu=2-5$ Hz) as a function of the hard color (5 - 10 keV)/(3 - 5 keV). These values were derived from the average PDS shown in Figure 9. While the QPO frequency decreases with increasing hard color, the %rms first decreases, then increases (see Table 9). There is a very strong anti-correlation between the hardness and the fractional rms variation of the QPO for the softest intervals, which inverts to a *correlation* for the hardest ranges, where the QPO frequency is ~ 2 Hz. Fractional rms variations extend up to $\sim 26\%$.

The VLFN component is represented by the best-fit power law (see Table 8 and Eqs. 1-4). The %rms values (integrated between 0.06-1 Hz) for all 6 hard color ranges are consistent with a constant value ($\sim 2\%$), except for the softest two intervals, where the 2σ upper-limits are $\leq 2.5\%$ and $\leq 2.4\%$ (Table 9), which were found by fixing the power law slope to 2.00.

High Frequency Noise. Data of type T3 were available for 34 bursts during the August 1985 observations. Each of these 34 burst peaks was divided in 16 second intervals, as described above. The FFTs were averaged together into a single PDS for each burst, and the Poisson level (fit as a constant) was subtracted. The %rms values were measured by summing the Poisson-level subtracted power for two frequency ranges: 10-100 Hz and 20-60 Hz. No significant HFN was seen in either the 10-100 Hz or 20-60 Hz frequency ranges. For the 10-100 Hz range 2σ upper limits were 6-12% with most values below 9%; for the 20-60 Hz range, 2σ upper limits were 5-10% with most values below 8%. When all FFTs from all bursts are summed into a single PDS, we find a %rms 2σ upper limits of 3.0% and 3.6% in

the 10-100 Hz and 20-60 Hz ranges, respectively.

We also separated the burst FFTs based on their instantaneous hardness and produced averaged PDS in the same hardness intervals used above. The FFTs in each hardness range were averaged together into a single PDS, and the Poisson level, calculated as described by Van der Klis (1988) was subtracted. The %rms values were calculated by summing the Poisson subtracted power over the relevant frequency range. The softest burst interval (hardness 0.74-0.80) had HFN with %rms 9.4 ± 2.7 and $10.8 \pm 3.6\%$ in the 20-60 Hz and 10-100 Hz frequency ranges, respectively, which we interpret as only marginally significant. No other individual energy spectral range produced a significant %rms, with typical 2σ upper limits in the range of 4-6% and 4-7% for the 20-60 Hz and 10-100 Hz frequency ranges, respectively.

4.2.2. Burst Timing Analysis: 1985 September 10 & 13

Power Density Spectra. We have investigated the timing behavior as a function of peak count-rate of the bursts observed during the 1985 September 10 & 13 data. Of the 541 bursts in this data set, 312 were observed using the high time resolution (2-4 ms) T3 OBC mode during periods without telemetry loss. These bursts were separated into three duration groups: $t_{dur} < 8s$, $8s < t_{dur} < 16s$, and $16s < t_{dur} < 32s$. There were no bursts longer than 32 seconds. For the purpose of this timing analysis, the burst “start” was defined as the first time bin which was 5σ (or greater) above the pre-burst background count rate; the burst “end” was defined as the first time bin that was 0.5σ below the pre-burst background count rate.

This criterion is different from that used to determine the period over which FFTs were taken for the August 1985 observations because of the very different time-evolution of the bursts during these observations; while the bursts observed during August 1985 were long (40 – 680s) and relatively flat-topped, the bursts during the September 1985 observations were short ($< 32s$) with a slowly decaying and “ringing” intensity profile (see Tan et al. 1991). Thus, we include the burst decay in the timing analysis of the September 1985 observations, while we could afford to exclude the burst decay in the timing analysis of the August 1985 observations. We caution that the shape of the PDS below ~ 1 Hz can be a strong function of the choices of “burst start” and “burst end” for a burst with a slowly decaying intensity profile, because the overall burst profile produces significant power at low frequencies.

After the bursts were separated according to their duration, one FFT was taken of each burst. The start-time of each FFT was taken 1 second after the burst “begin” (see above) to ensure that the rise of the burst, which can cause spurious spikes in the PDS, was not included in the FFT. Bursts of $t_{dur} < 8s$ had 8s FFTs; bursts of duration $8s < t_{dur} < 16s$, had 16s FFTs; and bursts of duration $16s < t_{dur} < 32s$ had 32s FFTs. The Nyquist frequency for all FFTs was 128 Hz. Because the QPO frequency varies strongly with peak count rate (Lubin et al. 1991), the FFTs were then grouped by the peak count rate

(see Figures 7d, e, i, & j) into three groups with roughly equal numbers of bursts in each: $I_{peak} < 1000\text{c/s}$, $1000 < I_{peak} < 1100\text{c/s}$, and $1100 < I_{peak} < 1500\text{c/s}$. PDS in the same countrate range but with different time durations were rebinned to the coarsest frequency resolution. These rebinned PDS were then averaged into a single PDS for each peak count rate range.

We account for differences between power due to random processes (*e.g.* noise features, QPO) and power due to deterministic processes (*i.e.* the burst envelope) by finding the frequency below which deterministic processes dominate the power spectrum and above which random process dominate. Fig. 10 shows results of an average PDS of 91 FFTs from bursts with duration $8\text{s} < t_{dur} < 16\text{s}$ and peak count rate $1000 < I_{peak} < 1100\text{c/s}$. Panel *a* shows the average power as a function of frequency. Panel *b* shows the ratio of σ/P as a function of frequency; here, $\sigma^2 = (\langle P^2 \rangle - \langle P \rangle^2)/N\text{FFTs}$ is the squared uncertainty in the mean power of all 91 FFTs as a function of frequency, and P is the mean power as a function of frequency. Panel *c* shows σ as a function of frequency. Down to frequencies of about 0.5 Hz, $\sigma \times \sqrt{N\text{FFTs}}$ is equal to the average power, indicating that the power spectrum is dominated by a random process. At lower frequencies, σ falls below this, as here the timing properties of the bursts are dominated by the deterministic burst envelope (see Van der Klis 1989).

We produced averaged PDS of the FFTs grouped by peak count rate, and one averaged PDS of all 312 FFTs (Fig. 11). In our fits to these PDS, we assumed a constant dead time induced Poisson level, which has been subtracted from the data, and rebinned the resulting PDS logarithmically.

Fractional rms Variations. Because the PDS below ~ 0.6 Hz are affected by the burst envelope, we used a two step modelling procedure (see Section 3.2., Equations 1-3) to separate the power due to the deterministic burst envelope and the random process. In the “primary” fit, we used the model $P(\nu) = P_{pl}(\nu) + P_{\text{const}}$ to fit the data at frequencies $\nu < 0.6$ Hz where the power is dominated by deterministic power and $\nu > 20$ Hz, where the power is assumed to be Poisson. We had attempted to subtract the deadtime-affected Poisson level, using the method described by Van der Klis (1989). Because of the significant intensity decay of the burst, the “constant count rate” assumption in the method described by Van der Klis (1989) is no longer valid, and we found that the Poisson level was over-estimated. We thus decided to assume a constant Poisson level and no measurable HFN. In the second step, we performed a “residual” fit, with the model $P(\nu) = P_{\text{pl, fixed}}(\nu) + P_{\text{const, fixed}} + P_{\text{pl}}(\nu) + P_{\text{Lor}}(\nu, \nu_c)$ to fit the data at frequencies $0.6\text{Hz} < \nu < 20\text{Hz}$, where $P_{\text{pl, fixed}}(\nu)$ and $P_{\text{const, fixed}}$ are the fixed values of the model from the “primary” fit. Figure 11 shows the 4 averaged PDS with their “composite” fit (*i.e.* the sum of both primary and residual fit).

The parameters derived from the primary and residual fit are given in Table 10. The χ^2 values are very high; the fits are poor, due largely to poor fitting in the 0.7-3 Hz frequency range. We attempted to fit models to the data with the 0.7-3 Hz range excluded, but the fits became highly unstable due to the interaction between the power-law and the Lorentzian parts of the fits. The primary power-law slopes are constant, independent of the peak count-rate, at $\alpha \sim 3.1$. The “residual” power-law slope in the lowest peak count-rate range was unconstrained, and destabilized the fit, so we fixed it to a mean value of the other

residual power-law slopes (which were in the range 0.7-0.9) to obtain an upper-limit on the “residual” VLFN power.

We confirm the previously reported correlation of the QPO centroid frequency with peak count rate in this peak intensity range found by Lubin et al. (1991) for this data set; however, note that at higher peak intensities, the relation has been found to be an *anti*-correlation (Tawara et al. 1982; Stella et al. 1988a; Lubin et al. 1991). Also, in these bursts, there appears to be an anti-correlation between QPO centroid frequency (or, burst peak count-rate) and QPO FWHM, which we measure as decreasing between the three count-rate ranges from 5, to 2, to 1 Hz. This anti-correlation is not globally observed from bursts in the Aug 28-29 and 30-31 1985 observations, with QPO frequencies in the range of 2-5 Hz (above) and Stella et al. (1988a) find a correlation between QPO centroid frequency and QPO FWHM in the individual Aug 1985 bursts.

The %rms values derived from the models are presented in Table 11 and have been corrected approximately for background, deadtime, and burst-duration, and changing burst intensity. We see no correlation between the burst peak intensity and the %rms values in either the primary power-law model, the residual power-law model. The sum of the primary and residual %rms is constant with increasing peak count rate at $\sim 50\%$. The %rms of the QPO appears to be anti-correlated to peak intensity decreasing from 21%, to 15% to 7% in the three different intensity ranges. However, we strongly caution against interpreting this data as indicating the existence of such an anti-correlation, due to the large systematic uncertainty caused by the extremely poor fits of the model to the data ($\chi^2/\nu \sim 10$). We attempted to overcome this by excluding the frequency region responsible for the poor fits (0.6-2 Hz, due to the burst “ringing”), however, this left the residual VLFN largely unconstrained. If we exclude the VLFN from these fits, the QPO %rms became very high, as the QPO FWHM broadened to compensate for the absence of a model at the low-frequency range. This systematic uncertainty accounts for the discrepancy between this result and Lubin et al. (1991), where the %rms of the QPO for bursts, separated by duration, were $\lesssim 10\%$ for about 2/3 of the duration ranges, and in the range 12-24% for the remaining 1/3 of the duration ranges.

5. The August 1985 Observations

Because of the richness of the 1985 August 28-29 & 30-31 observations we summarize and compare the spectral results of the bursts and PE in these data sets.

5.1. Spectral Results

5.1.1. *HIDs*

Figure 12 shows hardness-intensity diagrams (HIDs) of the bursts and the persistent emission for a soft color (3 - 5 keV/1 - 3 keV) (Figures 12a) and a hard color (5 - 10 keV/3 - 5 keV) (Figures 12b). The data points from the August 28-29 and August 30-31 observation are indicated with filled and open squares, respectively. For the burst data, each point in the HIDs represents an integration from the burst start to the burst end (see Section 4.1.). The bursts vary in duration from ~ 40 to 680 sec. For the persistent emission, each point represents an integration of 100 sec. The intensities are the *average* counting rates (1 - 20 keV) of each integration interval. All count rates have been normalized to the full array. Corrections for collimator transmission (aspect), background, and dead time (see Stella & Andrews 1985) have also been made.

In the HIDs, the bursts lie considerably away from the persistent emission, largely because of the difference in source intensity. There is also a great spectral difference between the bursts and the persistent emission, which is most plain in the soft ratio (3-5 keV/1-3 keV; Fig. 12a), where the bursts lie above the range of values occupied by the persistent emission. The spectral difference is not as great when considering the hard ratio (Fig. 12b), where there is considerable overlap in the parameter space of the bursts and persistent emission.

5.1.2. *CCDs*

Color-color diagrams (CCDs) were made of both the bursts and the persistent emission for each observation (Figure 13); all data from the two observations were used except when the nearby source 1728-34 was in the FOV (see Section 2.). The time intervals used to calculate the colors of the bursts and the persistent emission were the same as those described in Sec. 4.1.

In the CCD, the bursts clearly lie away from the PE, due largely, but not exclusively to the great difference in soft-ratio (3-5 keV/5-10 keV). The locus of of CCD points of the bursts is an elongated track, with one end roughly at the median hard-ratio of the persistent emission, but with a measureably higher soft-ratio, demonstrating the harder spectrum of the bursts compared to the persistent emission.

As with the persistent emission, the average burst hard color on August 30-31 is higher than on August 28-29. However, when one considers the soft color, the trends are *opposite* (*i.e.* the PE soft color is lower, while the burst soft color is higher).

5.2. Relation between Burst and Persistent Emission Hardness

We have investigated the possibility that the hardness of the bursts is correlated to that of the following persistent emission. Figure 14 shows the soft color (3 - 5 keV/1 - 3 keV) and the hard color (5 - 10 keV/3 - 5 keV) versus burst number. A solid point indicates the hardness of a burst while an open point indicates the hardness of the *following* persistent emission interval. (Some burst and persistent emission data could not be included due to telemetry losses or contamination by 1728-34.) A *global* correlation between burst and persistent emission hardness is most evident in the hard color (Figure 14b) where there is a clear drop in the hardness of both the bursts and the persistent emission between bursts # 28 and 40. (These bursts have the lowest peak counting rates and therefore the softest spectra; see Figures 12a,b.) The drop can not be attributed to the detector malfunction which occurred at burst #28, as the relevant experiment half was excluded from analysis; we also compared hardness ratios throughout the entire observation produced with only the experiment half which did not malfunction, and the global relation is still present.

There also exists a correlation between the burst spectrum and the persistent emission immediately following.

In Fig. 15, we show the burst hard color vs. that of the following PE, and the burst soft color vs. that of the following PE, separately for the Aug 28-29 (bursts 1-39) and Aug 30-31 (bursts 40-95) observations. Using a Spearman rank-order correlation, we find that, there exists a linear correlation between the burst hard and soft ratios that of the following persistent emission burst hard and soft ratios, with probabilities of such correlations being spuriously generated of $10^{-4} - 10^{-3}$. Thus, on both days, there is a measured correlation between the soft- and hard- color of the bursts and the following persistent emission on both days. Specifically, the correlation of the soft ratio of the burst and the following persistent emission is significant at 99.87% on Aug 28-29, and at 99.94% on Aug 30-31. The correlation between the hard ratio of the burst and the following persistent emission is significant at 99.96% on Aug 28-29, and at 99.99% on Aug 30-31. This demonstrates that the spectral hardness of the bursts is correlated with the following persistent emission.

We have shown (Sec. 5.1.2.; see Fig. 12 & Fig. 13) that, averaged over the entire observation, the PE and burst hard ratios both increase between Aug 28-29 and 30-31, but that the soft ratios follow opposite trends (decrease in the PE, increase in bursts). This may indicate that the emission of the PE and bursts in the 3-10 keV range are globally correlated, while that in the 1-3 keV range are either not correlated or possibly anti-correlated.

5.3. Comparison of the Strength of Variability in the Persistent Emission and Bursts

To graphically illustrate the differences between the timing properties of the PE and the bursts observed during the 1985 August observations, we plot in Fig. 16 the %rms values of the 2-5 Hz QPO in the bursts (see Section 4.2.1.; Table 9) and the PE (see

Section 3.2.2.1; Table 4) as a function of hardness ratio. The %rms of the QPO in the PE is generally correlated, while that of the bursts is anti-correlated. As for the VLFN, the %rms first increases, then decreases with decreasing hardness in the PE (see Table 4); in the bursts, however, the VLFN is constant in the harder ranges, and below detection in the softer ranges (see Table 9).

5.4. Relation between QPO Frequency and Burst Position on the HID

In Figure 17, using the HID in Figure 12b, we marked the location of each burst with an approximate QPO peak frequency, which was identified in averaged PDS of individual bursts. The frequency was estimated “by eye”, which required that a peak appeared to be significantly above the Poisson level in the 2-7 Hz range. This figure should be taken only to indicate somewhat qualitatively the timing behavior of bursts as a function of position on the HID. Bursts observed on August 28-29 are indicated by a circle, and bursts observed on Aug 30-31 are indicated by a square. Bursts where no QPO peak was identified are indicated on the HID with a dot inside the circle or square, and the circle or square was left empty when no PDS was available (*i.e.* the time resolution was poor or the burst was interrupted).

Motivated by what appears like two separate CCD branches, we somewhat arbitrarily separated the bursts on the HID into 5 separate groups indicated by the letters A-E. We averaged the FFTs from the bursts in these groups (produced as described in Section 4.2.1.) into single PDS, shown in Figure 18. Groups B & C, which correspond to roughly the same hardness range, have roughly identical PDS, with a small amount of VLFN and a sharp QPO peak at ~ 2 Hz. Groups A & D, which also correspond to roughly the same hardness range, have roughly identical PDS, with a small amount of VLFN and little or no indication of QPO in the 2-7 Hz range. Group E, the softest group, has a different QPO peak frequency (~ 5 Hz) than seen in the other groups. Thus, the PDS appear to be determined by the hardness of the burst, rather than the position on what appear to be branches.

We investigated the possibility of HFN correlated with position in the CCD. Using the available T3 data, we produced averaged PDS of FFTs from bursts in groups A, B, C, D, E, A+B, and D+E (see above). We attempted model fits to the PDS above 10 Hz using $P(\nu) = A_{\text{HFN}} \nu^{-\alpha} \exp(-\nu/\nu_{\text{cut-off}})$ (see HK89) but found the fits were unstable. We instead averaged the power in the ranges $20 \text{ Hz} < \nu < 60 \text{ Hz}$ and $10 \text{ Hz} < \nu < 100 \text{ Hz}$ for all 7 PDS. No HFN was detected with 2σ upper limits in the range 3-6%. The limits on the HFN in the PDS of A+B and D+E were 5.0% and 3.4% in the 10-100 Hz range and 4.7% and 4.1% in the 20-60 Hz range.

6. Discussion and Conclusions

Based on the combined X-ray spectral and fast-variability characteristics, two types of NS LMXB can be distinguished, the atoll and Z sources (HK89).

Atoll sources exhibit two states. The banana state is characterized by an upwardly curved branch in the CCD and power density spectra dominated by VLFN. The island state is characterized by lower X-ray intensities and little correlated motion in the CCD; its power density spectra are dominated by high frequency noise (HFN).

The Z sources are characterized by three branches in an X-ray color-color diagram: the horizontal, normal, and flaring branches– NB, HB, and FB. On the HB, these sources exhibit $\sim 13 - 55$ Hz QPO with a strong positive correlation between the QPO frequency and the source intensity. The strength of these QPO (fractional rms variations up to $\sim 8\%$) normally decreases with increasing source intensity. These QPO are accompanied by strong LFN whose strength (fractional rms variations up to $\sim 8\%$) has been reported to both increase (Cyg X-2; Hasinger 1991) and decrease (GX 5-1; Lewin et al. 1992) with increasing source intensity. On the normal branch (NB), QPO of $\sim 5 - 8$ Hz are observed; the frequency of these oscillations is approximately independent of source intensity, as is the strength of the VLFN component. The strength of both NB and HB QPO are strongly dependent on X-ray energy. Five of the Z sources (Sco X-1, GX 340+0, GX 17+2, Cyg X-2, and GX 349+2) exhibit a FB (Penninx et al. 1990b and references therein) whose characteristic properties merge smoothly with those of the NB. In the Flaring Branch (FB) all but GX 340+0 show QPO with frequencies of $\sim 10 - 20$ Hz which are highly correlated with X-ray intensity (HK89; Penninx et al. 1990a,b).

Overall, the CCD and fast-timing characteristics of the Rapid Burster bear no resemblance to those of either an atoll source or a Z-source.

6.1. The Persistent Emission

We found that the hard and soft ratios of the PE observed Aug 28-29 1985 are not statistically correlated, while those observed Aug 30-31 1985 are statistically correlated. The difference could be due to a lack of spectral variability on Aug 28-29.

In the PE alone, specifically in the August 1985 observations, the nature of the hard and soft colors looks similar to that seen in an atoll source island state (“by eye”; no correlation statistics exist for island states of atoll sources); however, spectral evolution of the magnitude observed in either an atoll or Z-source could go unnoticed in the August 1985 CCD, due to poor counting statistics. The highly peaked QPO (*i.e.* QPO power modelled by a function which has a very highly positive derivative over some frequency range) are unlike any timing characteristic in the PDS of atoll sources, most of which do not exhibit peaked QPO (however, 1608-522 has exhibited QPO; Yoshida et al. 1993). It is clear that the spectral hardness-correlated VLFN in the PE is related to the humps. It is also clear that the characteristics of the peaked QPO (%rms, width, centroid frequencies)

are independent of the hump; when the humps are excluded from the analysis, these characteristics and their spectral correlations do not change. Very globally, the QPO centroid frequencies increase with spectral hardness, the %rms first decreases and then increases, and the width of the QPO feature decreases (relative to the centroid frequency) during spectrally harder PE (Tables 3 & 4; Fig. 16).

An alternative view of the timing properties in the >1 Hz range may be to describe the QPO feature as HFN (such as is observed in atoll sources in the Island state) which becomes increasingly peaked as the energy spectrum hardens. In this view, the QPO of the persistent emission merges smoothly with the LFN, and thus the two could be of common origin.

No excess %rms in either the 10-100 or 20-60 Hz range (i.e. broad HFN) was found in the PE with 2σ upper limits of ~ 8 -10% (1-20 keV); these upper limits exceed the values measured for atoll sources; it cannot therefore be excluded that a HFN atoll-like feature is present in the PE in this frequency range.

The ~ 0.040 Hz QPO are found only in the (spectrally hard) humps, which sometimes occur following type II bursts. No sub-Hz QPO have been found in Z sources, and only one atoll source is known to exhibit sub-Hz QPO (1608-522, Yoshida et al. 1993; however, sub-Hz QPO has been observed in black-hole candidates – see, for a review, Tanaka & Lewin 1994 – and from several pulsars, see Takeshima et al. 1994 for a recent discussion). For the Rapid Burster, it is not unreasonable to assume that they are transient phenomena which are associated with the poorly understood accretion flow (see Lewin, Van Paradijs, & Taam 1993, and references therein).

6.2. The Bursts

The presence of QPO makes the RB during type II bursts very different from atoll sources. The behavior of the type II bursts of the Rapid Burster somewhat resembles that of Z sources. The CCDs of the long bursts appear as resolved “branches”. Like in the NB of Z sources, burst hardness is strongly correlated with source intensity (Kunieda et al. 1984; Tan et al. 1991; Lubin et al. 1992a; Figures 12a,b). The strength of the VLFN component in type II bursts is weakly correlated with spectral hardness (Tables 4 & 9). This behavior is somewhat similar to the NB in Z sources. Very globally, the QPO strength is anticorrelated with source intensity, as is true in both the HB and FB.

However, the Rapid Burster has striking differences from Z sources. The QPO frequency and peak flux in the Rapid Burster are anti-correlated (Lubin et al. 1991 and references therein); in Z sources, the QPO frequency is positively correlated with intensity (in both the HB and FB, where the QPO frequency is observed to change). If the “upper branch” in the burst CCD of the 1985 observation were to be interpreted as a Horizontal Branch, then the absence of LFN in Rapid Burster bursts (see Stella et al. 1988a) demonstrates that the burst QPO are unlike HB oscillations. Further, the frequencies observed in the Rapid Burster “Horizontal Branch” (2-3 Hz) are very different from those in the HB of Z

sources (13-55 Hz) – although we cannot rule out the existence of QPO at these frequencies, since the upper limits in the Rapid Burster are comparable to the measured strength in the Z sources’ HB (2-5% rms). There is also no evidence for broad HFN in the bursts, with 2σ upper-limits comparable to the HFN strength observed in the NB and HB of Z sources (~ 3 - 4%). Nothing resembling the Flaring Branch of a Z-source is observed.

6.3. A Comparison with Cir X-1

The Rapid Burster is not the only NS LMXB whose behavior is very different from atoll or Z sources; Cir X-1 also does not always behave clearly as one of these two classes, although at a certain orbital phase, it has been observed to behave like an atoll source (see Oosterbroek et al. 1994, hereafter O94). The temporal variations of Cir X-1 are very complicated (for a review, see e.g. Dower, Bradt & Morgan 1982). Cir X-1 emits type I X-ray bursts (Tennant, Fabian & Shafer 1986a,b), as does the Rapid Burster. QPO with centroid frequencies of 1.4 Hz and 5 - 18 Hz have been observed (Tennant 1987; 1988a,b). They occur in different spectral states. The frequency of the 1.4 Hz QPO changed by less than 5% as the source flux rose by a factor of 4. The 1.4 Hz QPO peak is remarkably narrow with a FWHM between 0.03 and 0.06 Hz. The 5 - 18 Hz QPO decreased in frequency with source intensity and appeared to saturate at a value of about 5.7 Hz. The latter resembles the flaring branch QPO in Z sources; however, the spectral hardness was strongly anti-correlated with the source intensity as the 5 - 18 Hz QPO occurred, and this is not observed in the flaring branch of most (but not all) Z sources.

The combined spectral and timing behavior of Cir X-1 has been investigated in depth by O94. Almost all of the observed spectral/timing behavior of Cir X-1 and the Rapid Burster are dissimilar; however, there is some similarity between the behavior of the Rapid Burster August 1985 PE and the zero-phase high-intensity observation (H in O94) of Cir X-1. During this observation, Cir X-1 had a very high intensity (~ 1500 *EXOSAT* c/s 1-20 keV). As the source spectrum hardened, the PDS evolved from VLFN only, to VLFN and a LFN broad-band component with a cut-off frequency of ~ 10 Hz, to broad LFN with peaked QPO near the cut-off frequency, to VLFN with peaked QPO at ~ 5 -7 Hz. The strength of the LFN and QPO summed together (~ 5 -7%) remained largely constant as a function of spectrum.

This is similar to the correlated spectral and timing behavior observed from the Rapid Burster when it exhibited PE in August 1985. During this observation there is some evidence for a VLFN component, accompanied by a broad timing component modelled by a Lorentzian which evolved into peaked QPO ($\nu_c \sim 3.0$ Hz) as the spectrum hardened (Tables 3 & 5; Figs. 5 & 6). However, if we were to interpret this to mean that the Rapid Burster is in a similar accretion state to Cir X-1, this would require that the Rapid Burster is near the Eddington limit during the persistent emission, as the behavior of Cir X-1 has been interpreted as being due to a near- or super-Eddington accretion rate (Van der Klis 1994). It seems unlikely that the PE should correspond to such a high accretion rate, as the type II bursts, which are cased by unstable accretion, have intensities which are a factor of

10 greater than the persistent emission intensity, with little or no observable LFN or VLFN, which is expected for Eddington and super-Eddington accretion (and observed in Z-source flaring branches, where super-Eddington accretion is thought to occur). Thus, while the changes of the PDS within with spectral hardness seen in the PE of the RB are similar to those seen in Cir X-1 at very high intensities, we do not interpret the Rapid Burster PE behavior as being due to \sim Eddington accretion.

A working hypothesis which classifies atoll sources, Z sources, black-hole candidates, and Cir X-1 has been suggested by Van der Klis (1994). He classifies the behavior of each in terms of differences in magnetic field strength (absent in BHCs, absent or weak in atoll sources, strong in Z sources) and accretion rate (which determines which state the source is in — low, high, or very high for BHCs; island or banana for atoll sources; HB, NB, or FB for Z sources). There is no obvious place to fit the Rapid Burster within this framework, neither when we consider the spectral and timing behavior of the PE or bursts separately, nor when they are considered together.

The spectral and timing behavior distinguishes the Rapid Burster from other NS low-mass X-ray binaries, including Cir X-1. The unknown mechanisms which drive the variability of its accretion rate clearly have significant effects on all facets of its appearance and behavior.

Acknowledgements

The authors would like to thank Victoria Scheribel and Jennifer Carson for aid in the preliminary data analysis. WHGL was supported by the United States National Aeronautics and Space Administration (NASA) under grant NAG8-700. JvP acknowledges support from NATO through grant RG 331/88. This paper is supported in part by the Netherlands Organization for Scientific Research (NWO) under grant PGS 78-277. LML acknowledges support of NASA through grant NGT-51295.

REFERENCES

- Alpar, M. A. & Shaham, J. 1985, *Nat*, **316**, 239
- Andrews, D., & Parmar, A., 1985, *EXOSAT Express*, **12**, 76
- Barr, P. White, N. E. Haberl, F., Stella, L., Pollard, G., Gottwald, M., & Parmar, A. N., 1987, *A&A*, **176**, 69
- Dotani, T. Proc. 23rd. ESLAB Symp. on Two Topics in X-ray Astronomy, Bologna, Italy, 13-20 September 1989 (ESA SP-296, Nov. 1989)
- Dotani, T., Mitsuda, K., Inoue, H., Tanaka, Y., Kawai, N., Tawara, Y., Makishima, K., van Paradijs, J., Penninx, W., Van der Klis, M., Tan, J., & Lewin, W.H.G, 1990, *ApJ***350**, 395
- Dower, R.G, Bradt, H.V., Morgan, E.H., 1982, *ApJ***261**, 228
- Hasinger, G., 1991, in : Particle Acceleration near Accreting Compact Objects, eds. J. van Paradijs, M. Van der Klis, A. Achterberg, North-Holland, Amsterdam, p. 23
- Hasinger, G., Van der Klis, M., 1989, *A&A*, **225**, 79
- Hoffman, J.A., Marshall, H.L & Lewin, W.H.G., 1978, *Nat*, **271**, 630
- Inoue, H. et al. 1980, *Nat*, **283**, 358
- Kawai, N., Matsuoka, M., Inoue, H., Ogawara, Y., Tanaka, Y., 1990, *PASJ***42**, 115
- Kleinmann, D.E., Kleinmann, S.G., Wright, E.L., 1976, *ApJ***210**, L83
- Kunieda, H., Tawara, Y., Hayakawa, S., Nagase, F., Inoue, H., Kawai, N., Makino, F., Makishima, K., Matsuoka, M., Murakami, T., Oda, M., Ogawara, Y., Ohashi, T., Shibazaki, N., Tanaka, Y., Kondo, I., Miyamoto, S., Tsunemi, H. & Yamashita, K. 1984, *PASJ***36**, 215

- Kunieda, H., Tawara, Y., 1990, PASJ**92**, 115
- Lamb, F. K., Shibazaki, N., Alpar, M.A., & Shaham J., 1985, Nat, **317**, 681
- Leahy, D.A., Darbro, W., Elsner, R.F., Weiskopf, M.C., Sutherland, P.C., Kahn, S.M., Grindlay, J.E., 1983, ApJ**266**, 160
- Lewin, W.H.G., Doty, J., Clark, G.W., Rappaport, S.A., Bradt, H.V.D., Doxsey, R., Hearn, D.R., Hoffman, J.A., Jernigan, J.G., Li, F.K., Mayer, W., McClintock, J., Primini, F., Richardson, J., 1976, ApJ**207**, L95
- Lewin, W.H.G., 1977, Amer. Sci., **65**, No. 5, p. 605
- Lewin, W.H.G., 1985, in : Galactic and Extragalactic Compact X-ray Sources, eds. Y. Tanaka & W.H.G. Lewin, Inst. of Space and Astronautical Sciences, Tokyo, p. 89
- Lewin, W.H.G., van Paradijs, J., & Van der Klis, M., 1988, Space Sci. Rev., **46**, 273
- Lewin, W.H.G., Lubin, L.M., Tan, J., Van der Klis, M., Van Paradijs, J., Penninx, W., Dotani, T., Mitsuda, K., 1992, MNRAS**256**, 545
- Lewin, W.H.G., Van Paradijs, J., Taam, R., 1993, Space Sci.Rev.**62**, 223
- Liller, W., 1977, ApJ**213**, L21
- Lubin, L.M., Stella, L., Lewin, W.H.G., Tan, J., Van Paradijs, J., Van der Klis, M., Penninx, W., 1991, MNRAS**249**, 300
- Lubin, L.M., Lewin, W.H.G., Dotani, T., Oosterbroek, T., Mitsuda, K., Magnier, E., van Paradijs, J., Van der Klis, M., 1992a, MNRAS**256**, 624
- Lubin, L.M., Lewin, W.H.G., Rutledge, R.E., Van Paradijs, J., Van der Klis, M., Stella, L., 1992b, MNRAS**258**, 759
- Lubin, L.M., Lewin, W.H.G., Van Paradijs, J., van der Klis, M., 1993, MNRAS**261**, 149L
- Marshall, H.L., Ulmer, M.P., Hoffman, J.A., Doty, J., Lewin, W.H.G., 1979, ApJ**227**, 555
- Oosterbroek, T., van der Klis, M., Kuulkers, E., Van Paradijs, V., and Lewin, W.H.G., 1994, A&A, submitted
- Penninx, W., Lewin, W.H.G., Mitsuda, K., Van der Klis, van Paradijs, J., Zijlstra, A.A., 1991a, MNRAS**243**, 114
- Penninx, W., Lewin, W.H.G., Tan, J., Mitsuda, K., Van der Klis, van Paradijs, J., 1991b, MNRAS**249**, 113
- Rutledge, R.E., Lewin, W.H.G., Lubin, L.M., Oosterbroek, T., Van Paradijs, J., Van der Klis, M., Dotani, T., 1995, in preparation
- Stella, L., Andrews, D., 1985, EXOSAT Express, No. 10, p. 35

- Stella, L., Haberl, F., Lewin, W.H.G., Parmar, A., White, N.E., van Paradijs, J., 1988a, *ApJ***324**, 379
- Stella, L., Haberl, F., Lewin, W.H.G., Parmar, A., Van der Klis, M., Van Paradijs, J., 1988b, *ApJ***327**, L13
- Takeshima, T., et al. , 1994, *ApJ***436**, 871
- Tanaka, Y., & Lewin, W.H.G., 1994 in: “X-ray Binaries”, eds. W. Lewin, J. v. Paradijs, & E. v.d. Heuvel, Cambridge Univ. Press, in press
- Tan, J., Lewin, W.H.G., Lubin, L.M., Van Paradijs, J., Penninx, W., Van der Klis, M., Damen, E., Stella, L., 1991, *MNRAS***251**, 1
- Tawara, Y., Hayakawa, S., Kunieda, H., Makino, F., Nagase, F., 1982, *Nat*, **299**, 38
- Tennant, A.F., Fabian, A.C., & Shafer, R.A. 1986a, *MNRAS***219**, 871
- Tennant, A.F., Fabian, A.C., & Shafer, R.A., 1986b, *MNRAS***221**, 27P
- Tennant, A.F., 1987, *MNRAS***226**, 971
- Tennant, A.F., 1988a, *MNRAS***230**, 403
- Tennant, A.F., 1988b, in : The Physics of Compact Objects : Theory Versus Observations, eds. L. Filipov, N.E. White, COSPAR/IAU Symp., Sofia, July 1987, Pergamon, London
- Turner, M.J.L., Smith, A., Zimmermann, H.U., 1981, *Space Sci.Rev.***30**, 513
- Turner, M.J.L., et al. , 1989, *PASJ***41**, 345 513
- Van der Klis, M. 1989, in : Timing Neutron Stars, eds. H. Ögelman, E.P.J. Van den Heuvel, Kluwer Academic Publ., p. 27
- Van der Klis, M. 1994, *ApJS***92**, 511
- Van Paradijs, Cominsky, L., Lewin, W.H.G., 1979, *MNRAS***189**, 387
- White, N.E., Mason, K.O., Carpenter, G.F., Skinner, G.K., 1978, *MNRAS***184**, 1P
- Yoshida, K., Mitsuda, K., Ebisawa, K., Ueda, Y., Fujimoto, R., Yaqoob, T., and Done, C., 1993, *PASJ***45**, 605

Table 1: Observational Data

Date	Period (UT)	OBC Modes ^a	Energy Channels	Time Resolution (ms)	Transmission ^b (%)
1983 Aug 15 ^d	00:57 - 09:59	E4	8	93.75	14
1984 Jul 17	00:50 - 06:17	E5	32	312.5	17.5
1985 Aug 28-29 ^d	17:47 - 8:12	E5	8, 32	312.5, 156.25, 93.75	42
		I5	1	31.25	
		T3	1	3.9	
1985 Aug 30-31 ^d	18:28 - 7:24	E5	64	1000	40.25, 23, 17.25 ^c
		I5	1	31.25	
		I7	1, 4	0.98, 3.9, 7.8	
		T3	1	3.9	
1985 Sept 10	12:10 - 18:22	E5	64	500, 750	43
		T3	1	1.95, 3.9	
1985 Sept 13	02:55 - 10:45	E5	64	750	43
		T3	1	3.9	

^aNot all OBC modes are available during the whole observation; “E5”=HER5; “I5”=HER5 (no energy resolution; “T3”=HTR3

^bIncludes aspect efficiency and correction to full array area

^cDetector halves swapped on and off source; see Sec. 2.

^dPersistent emission detected during these observations

Table 2: Counts Conversions

I7 range (keV)	to	E5 range (keV)	slope (\pm ; E5 Counts/I7 Counts)	intercept (\pm ; E5 Counts)
Persistent Emission				
1.2-3.4		0.9-2.6	0.55 ± 0.02	0.62 ± 0.53
3.7-5.5		2.9-4.7	1.02 ± 0.017	2.36 ± 0.44
5.8-10.3		5.0-6.9	0.92 ± 0.024	1.91 ± 0.43
Bursts				
1.2-3.4		0.9-2.6	0.48 ± 0.009	3.6 ± 1.5
3.7-5.5		2.9-4.7	0.98 ± 0.007	6.5 ± 1.5
5.8-10.3		5.0-6.9	1.02 ± 0.008	4.4 ± 1.1

Table 3: August 1985 Persistent Emission PDS Fit Parameters

Hard Color	χ^2 (dof)	α	$\nu_{0.04Hz}$	$\Gamma_{0.04Hz}$	ν_1	Γ_1	ν_2	Γ_2
0.66-0.74	78 (50)	-	-	-	$0.075^{+0.44}_{-1.1}$	$2.9^{+0.7}_{-0.6}$	-	-
0.74-0.78	48 (50)	2.0 ± 0.3	-	-	$-1.1^{+1.6}_{-2.5}$	$10^{+1.4}_{-1.2}$	-	-
0.78-0.82	83 (50)	1.0 ± 0.1	-	-	2.8 ± 0.1	1.6 ± 0.2	-	-
0.82-0.86	62 (49)	2.1 ± 0.2	0.041^a	0.0011^a	2.1 ± 0.2	$5.2^{+0.6}_{-0.5}$	-	-
0.86-0.90	64 (44)	2.3 ± 0.3	0.040 ± 0.03	$0.0016^{+0.011}_{-0.007}$	2.49 ± 0.04	$0.56^{+0.09}_{-0.07}$	3.57 ± 0.05	0.7 ± 0.1
0.90-1.02	58 (44)	1.28 ± 0.04	0.0427 ± 0.0007	0.0010 ± 0.0004	2.88 ± 0.02	$0.33^{+0.08}_{-0.11}$	3.97 ± 0.05	1.2 ± 0.06

^a Values were fixed

Table 4: August 1985 Persistent Emission % rms Values from Parametric Fits

Hard Color	VLFN ^a % rms	QPO (~ 0.04 Hz) % rms	QPO (ν_1) % rms	QPO (ν_2) % rms	QPO($\nu_1 + \nu_2$) % rms
0.66-0.74	$\leq 2.9^b$	-	14 ± 2	-	14 ± 2
0.74-0.78	5.6 ± 0.8	-	$16.6^{+1.0}_{-1.5}$	-	$16.6^{+1.0}_{-1.5}$
0.78-0.82	7.1 ± 0.4	-	$12.0^{+0.6}_{-0.8}$	-	$12.0^{+0.6}_{-0.8}$
0.82-0.86	7.4 ± 0.6	$\leq 2.5^b$	17.4 ± 0.7	-	17.4 ± 0.7
0.86-0.90	$10.2^{+1.5}_{-2.0}$	6.9 ± 1.3	11.4 ± 0.9	12.7 ± 0.9	17.1 ± 1.9
0.90-1.02	17.5 ± 0.7	$\leq 84^{b,c}$	$14.0^{+0.9}_{-1.7}$	$22.2^{+0.4}_{-1.1}$	$26.2^{+1.7}_{-3.4}$

^a Integrated from 0.0078-1.0 Hz

^b 2σ upper limits

^c Poorly constrained due to poor frequency resolution

Table 5: August 1985 Persistent Emission PDS Fit Parameters (Hump Excluded)

Hard Color	χ^2 (dof)	α	ν	Γ	ν	Γ
0.66-0.74	70 (52)	2.00^a	0.6 ± 0.2	$1.6^{+0.4}_{-0.3}$	-	-
0.74-0.78	60 (52)	$2.6^{+0.8}_{-0.6}$	$0.1^{+0.4}_{-0.5}$	$4.73^{+0.9}_{-0.6}$	-	-
0.78-0.82	77 (52)	-	2.7 ± 0.1	1.8 ± 0.2	-	-
0.82-0.86	53 (52)	2.5 ± 0.1	1.8 ± 0.2	4.5 ± 0.4	-	-
0.86-0.90	110 (49)	2.8 ± 0.1	2.45 ± 0.05	0.48 ± 0.07	3.43 ± 0.06	0.6 ± 0.2
0.90-1.02	84 (52)	1.77 ± 0.02	3.42 ± 0.03	0.53 ± 0.09	-	-

^a Value fixed

Table 6: August 1985 Persistent Emission % rms Values from Parametric Fits (Hump Excluded)

Hard Color	VLFN ^a % rms	QPO ($\nu_1 + \nu_2$) % rms (0.01-100 Hz)
0.66-0.74	$\leq 2.2^b$	12.7 ± 2.7
0.74-0.78	$\leq 4.4^b$	$15.9^{+1.8}_{-2.3}$
0.78-0.82	$2.8^{+0.9}_{-0.7}$	$15.3^{+2.8}_{-3.1}$
0.82-0.86	$4.4^{+0.7}_{-0.8}$	$16.4^{+1.2}_{-1.9}$
0.86-0.90	$7.5^{+1.4}_{-1.8}$	$16.7^{+1.0}_{-1.5}$
0.90-1.02	$3.5^{+0.6}_{-0.6}$	$20.4^{+0.9}_{-0.8}$

^a Integrated from 0.0078-1.0 Hz

^b 2σ upper limits

Table 7: Weighted Average Type II Burst Hardness Ratios

Date	3-5 keV/ 1-3 keV	5-10 keV/ 3-5 keV
1984 Jul 17	3.09 ± 0.04	0.998 ± 0.007
1985 Aug 28-29	2.93 ± 0.03	0.94 ± 0.01
1985 Aug 30-31	2.98 ± 0.01	0.99 ± 0.01
1985 Sep 10	2.88 ± 0.01	0.943 ± 0.003
1985 Sep 13	2.77 ± 0.01	0.892 ± 0.003

Table 8: August 1985 Burst Fit Parameters

Hard Color	χ^2 (dof)	α	ν_1	Γ_1	ν_2	Γ_2
0.74-0.80	60 (49)	2.00^a	4.71 ± 0.04	0.89 ± 0.08	-	-
0.80-0.86	50 (49)	2.00^a	4.87 ± 0.02	0.67 ± 0.04	-	-
0.86-0.92	57 (49)	1.8 ± 0.3	4.83 ± 0.03	0.85 ± 0.07	-	-
0.92-0.98	32 (49)	1.4 ± 0.2	4.45 ± 0.14	1.7 ± 0.3	-	-
0.98-1.04	53 (49)	1.8 ± 0.2	2.20 ± 0.04	$0.43^{+0.16}_{-0.08}$	-	-
1.04-1.12	40 (46)	2.2 ± 0.3	2.03 ± 0.05	0.08 ± 0.02	2.36 ± 0.03	0.36 ± 0.06

^a Fixed

Table 9: August 1985 Burst % rms Values from Parametric Fits

Hardness	VLFN ^a % rms	QPO ($\nu_1 + \nu_2$) % rms
0.74-0.80	$\leq 2.5^b$	25.6 ± 0.9
0.80-0.86	$\leq 2.4^b$	$21.2^{+1.3}_{-0.2}$
0.86-0.92	2.0 ± 0.6	$14.0^{+1.3}_{-0.1}$
0.92-0.98	2.2 ± 0.3	5.8 ± 0.4
0.98-1.04	2.3 ± 0.3	4.6 ± 0.4
1.04-1.12	2.3 ± 0.3	$10.7^{+7.6}_{-1.1}$

^a Integrated from 0.06-1.0 Hz

^b Upper limits are 2σ confidence

^c Sum of two fitted Lorentzians

Table 10: September 1985 Bursts PDS Fit Parameters

Peak Count Rate ^a (counts/sec)	Primary ^b Fit		Residual Fit			
	χ^2 (dof)	VLFN	χ^2 (dof)	VLFN	QPO	
		α		α	ν_c (Hz)	Γ (Hz)
$300 < I_{peak} < 1000$	18.3 (15)	3.05 ± 0.02	248 (21)	0.8^c	3.97 ± 0.2	$5^{+0.6}_{-0.2}$
$1000 < I_{peak} < 1100$	56.2 (15)	3.13 ± 0.02	192 (21)	$0.7^{+0.3}_{-0.1}$	5.08 ± 0.09	2.52 ± 0.2
$1100 < I_{peak} < 1500$	30.3 (15)	3.08 ± 0.02	84 (21)	0.73 ± 0.05	5.82 ± 0.03	0.96 ± 0.15
All	62.6 (15)	3.11 ± 0.01	363 (21)	0.91 ± 0.07	5.19 ± 0.07	2.7 ± 0.2

^a Corrected to full detector area and for aspect, but not deadtime

^b Power law fit above 0.6 Hz

^c Value Fixed

Table 11: September 1985 Bursts Parametric Fit Results

Peak Count Rate ^a (counts/sec)	Primary ^b VLFN ^c % rms	Residual VLFN ^c % rms	Primary + Residual VLFN ^c % rms	QPO % rms
$300 < I_{peak} < 1000$	52 ± 2	$< 6.7^d$	53 ± 2	21 ± 1.0
$1000 < I_{peak} < 1100$	48 ± 2	4.4 ± 0.4	48 ± 2	15.5 ± 0.7
$1100 < I_{peak} < 1500$	52 ± 2	6.9 ± 0.5	52 ± 2	7.6 ± 0.5
All	50 ± 2	7.5 ± 0.5	51 ± 2	13.9 ± 0.7

^a Corrected to full detector area and for aspect, but not deadtime

^b Power law fit above 0.6 Hz

^c Integrated from 0.125-1.0 Hz

^d Upper limits are 2σ

Fig. 1.— HIDs and CCD for the persistent emission observed 15 Aug 1983 (type I bursts were excluded). The count rates have been background subtracted, aspect corrected, and normalized to the full array. No dead time corrections (which are $\simeq 1\%$) have been performed. Because of a different OBC mode, the energy ranges used in the analysis of this observation were different from those used in the other observations, which complicates a direct comparison between these HIDs and CCDs and those of other observations. Each point in all three panels represents 600 seconds of integration. a) HID, 2-17 keV count rate vs. soft color (5.7–9.3 keV/2.0–5.7 keV). b) HID, 2-17 keV count rate vs hard color (9.3–17.0 keV/5.7–9.3 keV). c) Color-color diagram. soft color vs. hard color.

Fig. 2.— HIDs and CCD for the persistent emission observed 28-29 Aug 1985 and 30-31 Aug 1985. The observation date is indicated at the top of each panel. The count rates have been background subtracted, dead time corrected, aspect corrected, and normalized to the full array. An average 1-sigma error bar is included in each panel. a) 28-29 Aug 1985 HID, 1-20 keV count rate vs. hard color. b) 28-29 Aug 1985 HID, 1-20 keV count rate vs. soft color. c) 28-29 Aug 1985 CCD, soft color vs. hard color. d) 30-31 Aug 1985 HID, 1-20 keV count rate vs. hard color. e) 30-31 Aug 1985 HID, 1-20 keV count rate vs. soft color. f) 30-31 Aug 1985 CCD, soft color vs. hard color.

Fig. 3.— Distribution of the average (1 - 20 keV) intensities (a) and the soft (3 - 5 keV/1 - 3 keV) (b) and hard color (5 - 10 keV/3 - 5 keV) (c) of the persistent emission intervals from the two Aug 1985 data sets. The integration time for each point was 100 sec. All count rates corrected for aspect, dead time (see Stella & Andrews 1985; Eq. 3.10 of Van der Klis 1989), and normalized to the full array area. The persistent emission observed during the August 30-31 observation is clearly *harder* than that on August 28-29 (panel c) in the hard color, while it is *softer* in the soft color.

Fig. 4.— PDS of PE observed during the 1983 observations. The included energy range was 2-12 keV. The 12 FFTs were each 1536 sec long, with a Nyquist Frequency of 5.6 Hz. The FFTs were summed into a single PDS, which was logarithmically rebinned. Panels show the averaged PDS of these hardness bins, and the averaged PDS of all FFTs together. There is no obvious VLFN in any of these PDS. 2σ upper limits in VLFN for the PDS of all 215 FFTs in the frequency range 0.005-1.0 Hz is 2.0%.

Fig. 5.— Averaged PDS and best fit model of the persistent emission during the 1985 August 28-29 & 30-31 observations for six ranges of the hard color (5 - 10 keV/3 - 5 keV). The range of the hard color and the number of FFTs in this range are indicated in the upper right of each panel. The best fit Poisson level has been subtracted, and the PDS has been logarithmically rebinned. The filled squares with arrows pointing downwards indicate 2σ upper limits. The line is the best fit model to all data points (including those consistent with zero power). The frequency of the QPO peak increases with increasing hardness. The ~ 40 mHz oscillations are only present in the portions of persistent emission which are relatively hard (panels e,f).

Fig. 6.— Averaged PDS and best fit model of the persistent emission during the 1985 August 28-29 & 30-31 observations for six ranges of the hard color (5 - 10 keV/3 - 5 keV), excluding the first 256 sec of PE (*i.e.* the “hump”). The range of the hard color and the number of FFTs in this range are indicated in the upper right of each panel. The best fit Poisson level has been subtracted, and the PDS has been logarithmically rebinned. The filled squares with arrows pointing downwards indicate 2σ upper limits. The line is the best fit model to all data points (including those consistent with zero power).

Fig. 7.— HIDs and CCDs of type II bursts observed in 5 of the 6 observation periods of the Rapid Burster with the *EXOSAT* ME instrument. This figure shows all type II bursts which were observed with ≥ 4 energy channels by the *EXOSAT* ME instrument. The 1-20 keV peak count rates (in counts/sec) are averaged over ~ 1 sec, are corrected for dead time (see Stella & Andrews 1985) and aspect, and are normalized to the full array. Each panel contains an average error bar in the upper right-hand corner. The observation date is indicated at the top of each column of panels. Note that $1 \text{ count/s} \simeq 1.6 \times 10^{-11} \text{ ergs cm}^{-2} \text{ s}^{-1}$; see Tan et al. (1991).

Fig. 8.— Composite HIDs and CCD of type II bursts observed by EXOSAT. The legend in the figure indicates the observation period for each data point. All count rates are corrected for deadtime, aspect, and normalized to the full EXOSAT ME array area. The July 1984 and September 1985 data points represent the average hardnesses of the (≥ 10) bursts in a peak count rate range indicated by the horizontal bars. The 1σ errors in mean hardness for the July, 1984 and September, 1985 data are indicated in each point, assuming the burst hardnesses in each peak count rate range are normally distributed. An average 1σ error bar is included on one point for the August 28-29 and 30-31, 1985 data. a) Soft color vs. burst peak count rate (c/s). b) Hard color vs. burst peak count rate (c/s). c) Hard color vs. soft color.

Fig. 9.— Averaged PDS, logarithmically rebinned, of the type II bursts during the 1985 August 28-29 & 30-31 observations for six ranges of the hard color (5 - 10 keV/3 - 5 keV). The solid lines indicate the best fit models (Table 8). The number of FFTs and the range of hardness of each averaged PDS are indicated in the upper left of each panel. The QPO frequency decreases from ~ 5 Hz to ~ 2 Hz with increasing hard color while the % rms in the QPO at first decreases, and then increases with increasing hard color.

Fig. 10.— Comparison of signal power with Poisson power. (a) PDS from 91 burst FFTs (from Sept. 10-13 1985) using T3 data. The Poisson level was not subtracted from the power. (b) The ratio of σ at each frequency to the power at each frequency. (c) The uncertainty in the mean power (σ) at each frequency, which is found from the scatter of the 91 different powers from the 91 different FFTs at each frequency. The divergence of the ratio of σ/Power from $1/(\text{NFFT})^{1/2}$ at frequencies below 0.5 Hz demonstrates that the power at these frequencies is largely deterministic.

Fig. 11.— PDS of 312 type II bursts observed September 10-13, 1985 using OBC mode T3. Solid lines indicate the sum of the Primary and Residual models (see text). The bursts were separated by peak intensity, which was measured in ~ 1 sec bins, corrected to the full array area for aspect, but not for deadtime. Error bars are 1σ , while the upper limits are 2σ . Solid symbols with arrows pointing downwards indicate 2σ upper limits. **(a)** Averaged PDS of FFTs from 100 bursts with peak intensity below 1000 c/s. **(b)** Averaged PDS of FFTs from 116 bursts with peak intensity between 1000 and 1100 c/s. **(c)** Averaged PDS of FFTs from 96 bursts with peak intensity above 1100 c/s. **(d)** Averaged PDS of all 312 bursts.

Fig. 12.— Hardness-intensity diagrams (HIDs) of the bursts and the persistent emission for the soft ratio (3 - 5 keV/1 - 3 keV) [(a)] and the hard ratio (5 - 10 keV/3 - 5 keV) [(b)]. The data points from the August 28-29 and August 30-31, 1985 observations are indicated with closed and open symbols, respectively. For the burst data, each point represents a single burst. For the persistent emission data, each point represents an integration of 100 sec. For the bursts, $1 \text{ count/s} \simeq 1.6 \times 10^{-11} \text{ ergs cm}^{-2} \text{ s}^{-1}$; for the persistent emission, $1 \text{ count/s} \simeq 7.8 \times 10^{-12} \text{ ergs cm}^{-2} \text{ s}^{-1}$ (see Tan et al. 1991). All count rates have been normalized to the full array area. Corrections for collimator transmission (aspect), background, and dead time (see Stella & Andrews 1985) have also been made. A sample error bar is shown, offset from the data, separately for the persistent emission and the bursts. The previously reported correlation between burst peak counting rate and hardness (or equivalently temperature) is apparent.

Fig. 13.— The composite CCD for bursts and persistent emission during the August 28-29 and August 30-31, 1985 observations. The bursts observed on August 28-29 and August 30-31 are indicated by closed and open squares, respectively. For bursts, each data point represents a single burst. The persistent emission observed on August 28-29 and August 30-31 are indicated by closed and open triangles, respectively. Each data point represents an integration of 100 sec. A sample error bar for the burst and the persistent emission data is shown on one data point.

Fig. 14.— a) The soft color (3 - 5 keV/1 - 3 keV) and b) the hard color (5 - 10 keV/3 - 5 keV) versus burst number. All bursts are numbered sequentially in accordance with the numbering of Stella et al. (1988a) and Lubin et al. (1992b). Solid and open points indicate the hardness of the burst and the *following* persistent emission interval, respectively. (Some of the bursts and persistent emission data could not be included due to telemetry losses and the contamination of the nearby source 1728-34.) A global correlation between the hardness of the bursts and the persistent emission is most evident in the hard ratio (b).

Fig. 15.— The hardness ratios of the bursts versus those of the *following* persistent emission interval; the soft color (3 - 5 keV/1 - 3 keV) for the August 28-29 (a) and 30-31 (b) observation and the hard color (5 - 10 keV/3 - 5 keV) for the August 28-29 (c) and 30-31 (d) observations. There are statistical correlations in all four comparisons, with a probability of being generated from uncorrelated data of: (a) 0.13%, (b) 0.06%, (c) 0.04%, and (d) 0.01% (see text).

Fig. 16.— Comparison of the % rms values for bursts and persistent emission (PE) in the 1985 August 28-29 and 30-31 observations with the PE “humps” excluded. Error bars are 1σ for the %rms and indicate the hardness range for the hardness ratio. Upper-limits are 2σ . **(a)** %rms values of the 2-5 Hz QPO as a function of hardness interval for PE and bursts. The trends of %rms for the PE and bursts are oppositely directed. **(b)** %rms of the VLFN in the PE and bursts.

Fig. 17.— HID of bursts observed during August 1985 (hard color vs. 1-20 keV count rate). Aug 28-29 bursts are indicated by a circle; Aug 30-31 bursts are indicated by a square. Bursts which had a QPO peak between 2-7 Hz which could be identified by eye have the approximate centroid frequency indicated at each point. Dots indicate that no QPO was seen. No mark indicates that a complete PDS is not available. The broken lines divide the HID into groups of bursts, separating roughly along the separate “branches” (arbitrarily drawn), labelled A, B, C, D, & E as indicated. An average error bar is included in the bottom right corner.

Fig. 18.— PDS of August 1985 bursts grouped as indicated in Figure 17. The group is indicated in the upper left corner. The PDS panels are ordered on the figure roughly as the corresponding position on the HID in Figure 17. Error bars for the power are included on each point. The Poisson level has not been subtracted off, and the data have been logarithmically rebinned.

15 Aug 1983: Persistent Emission

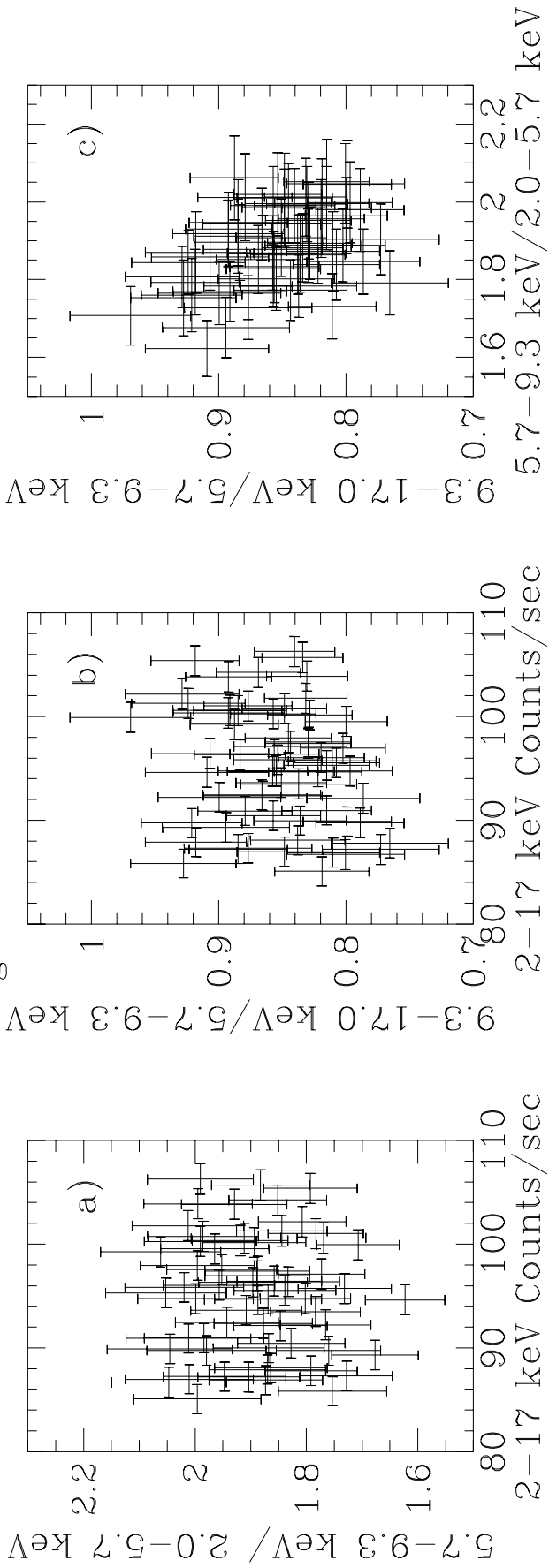


Figure 1

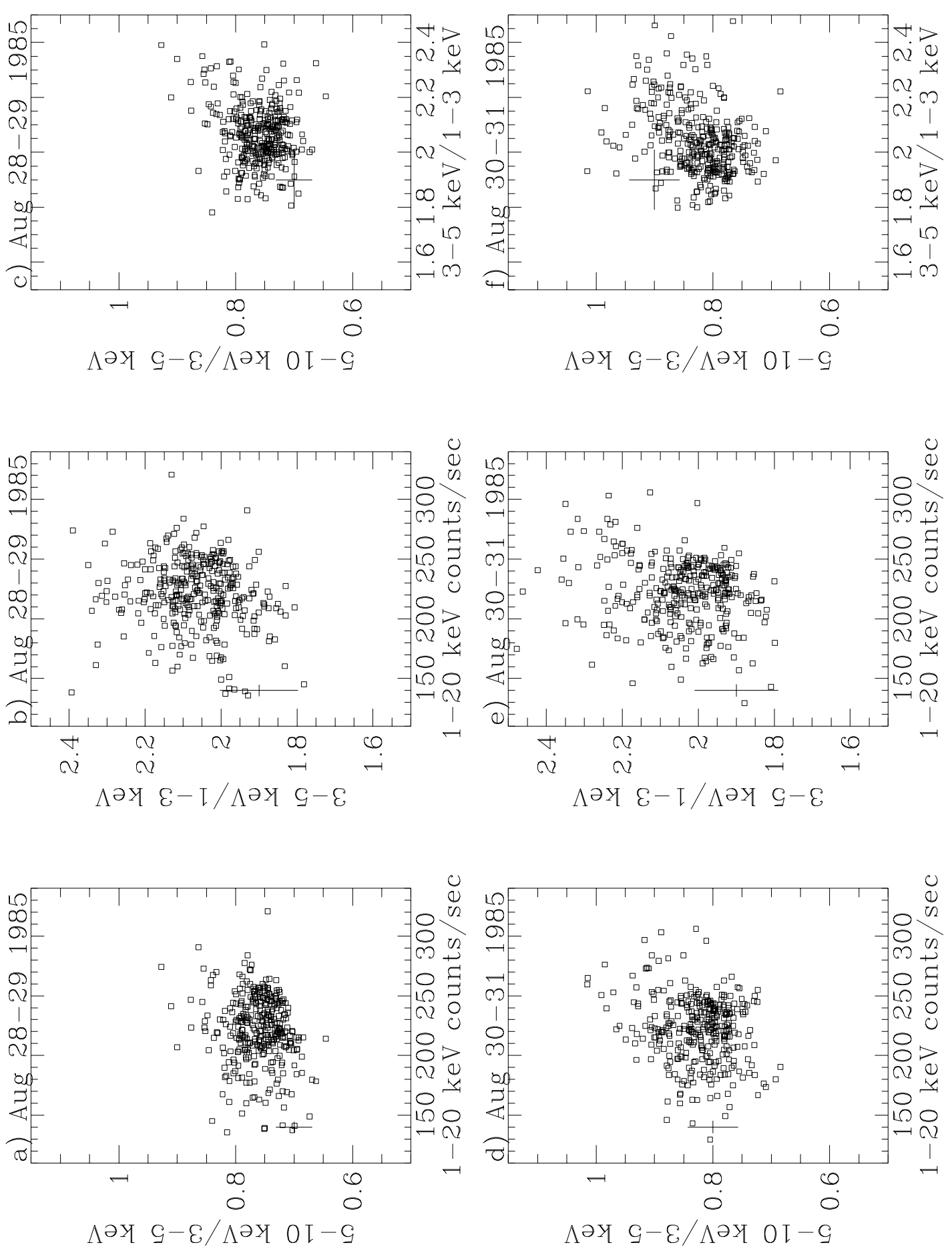


Figure 2

PERSISTENT EMISSION

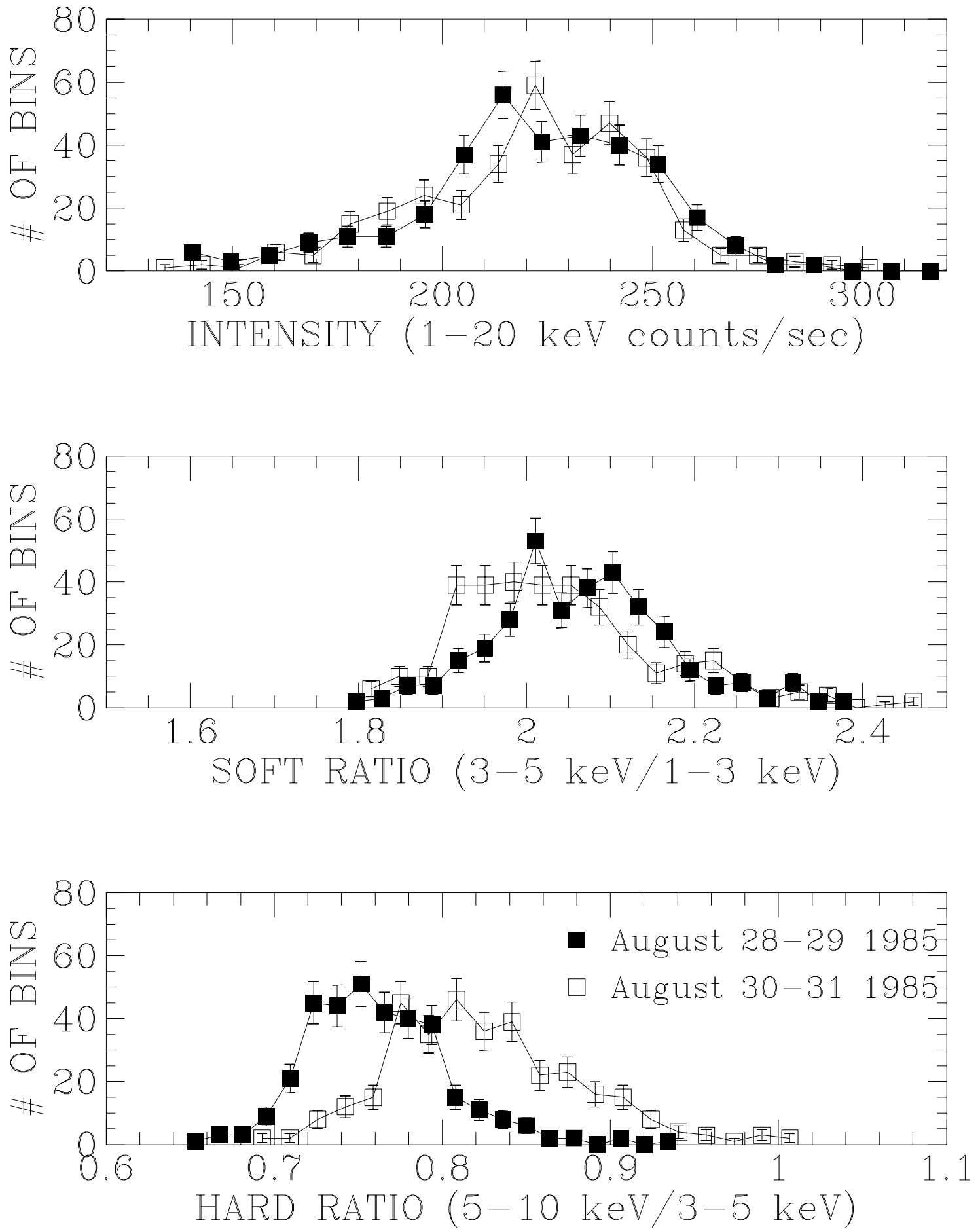


Figure 3

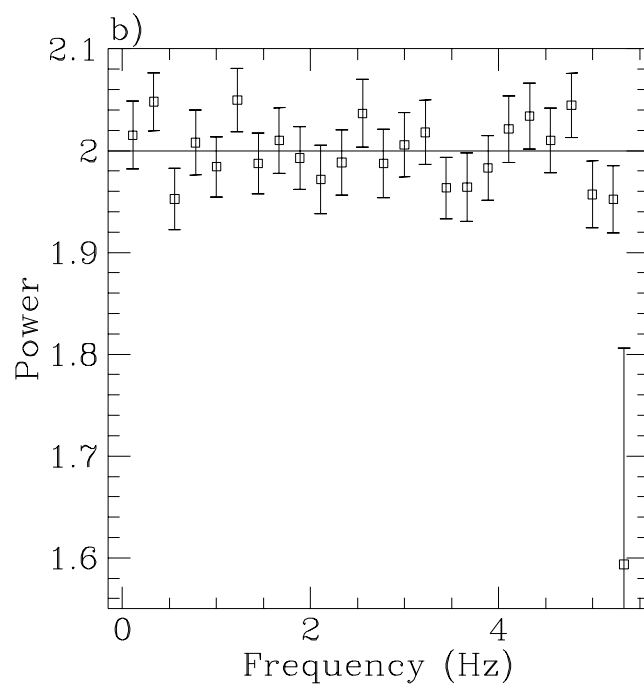
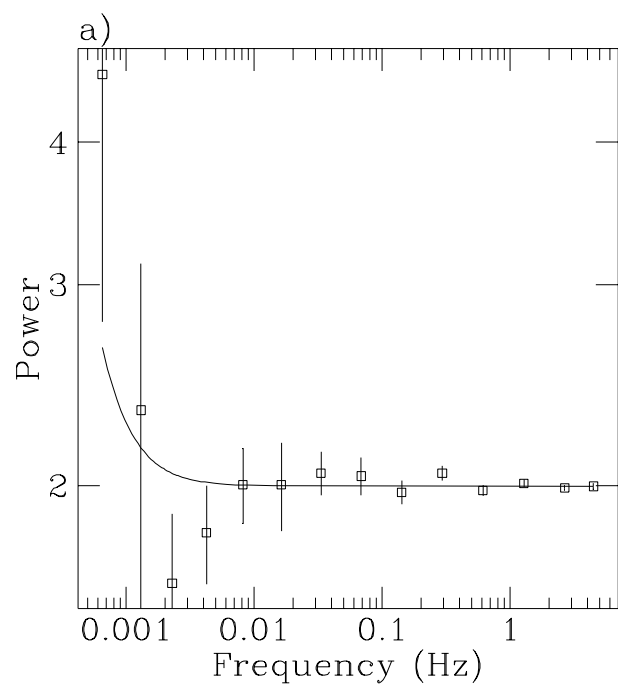


Figure 4

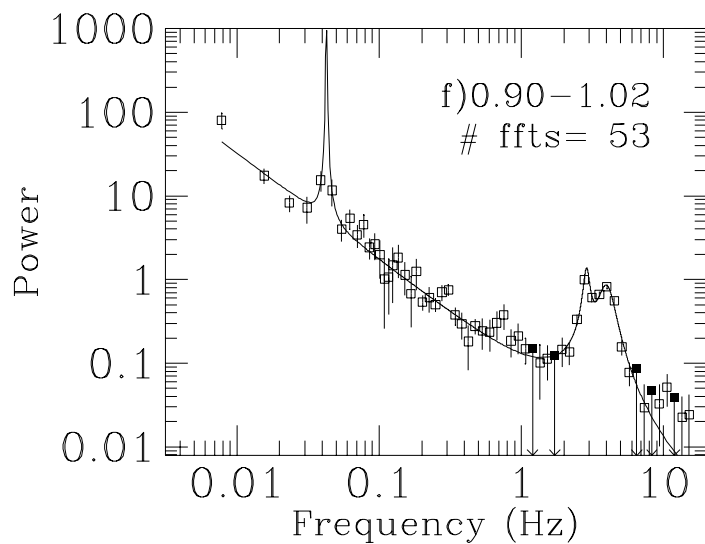
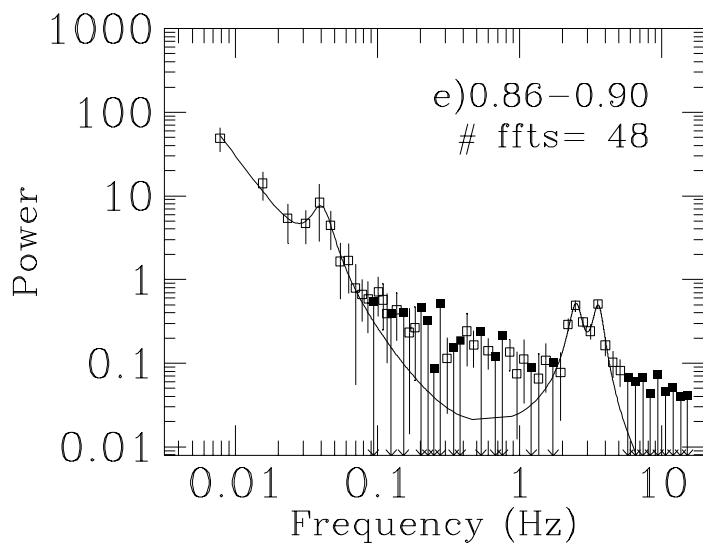
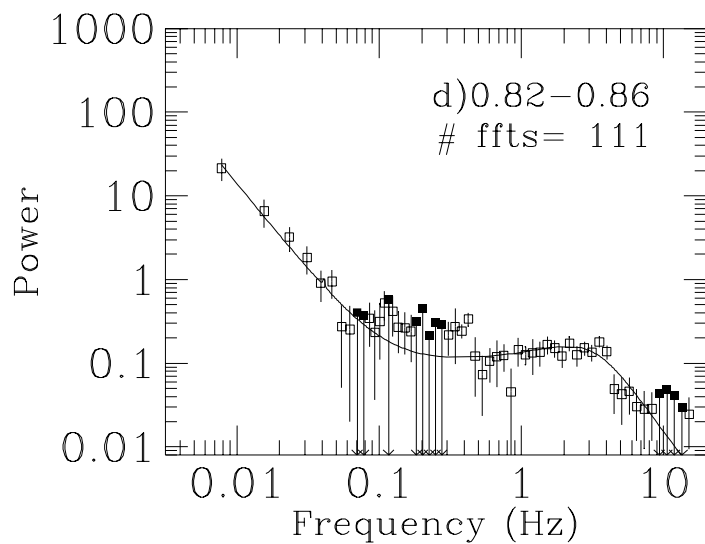
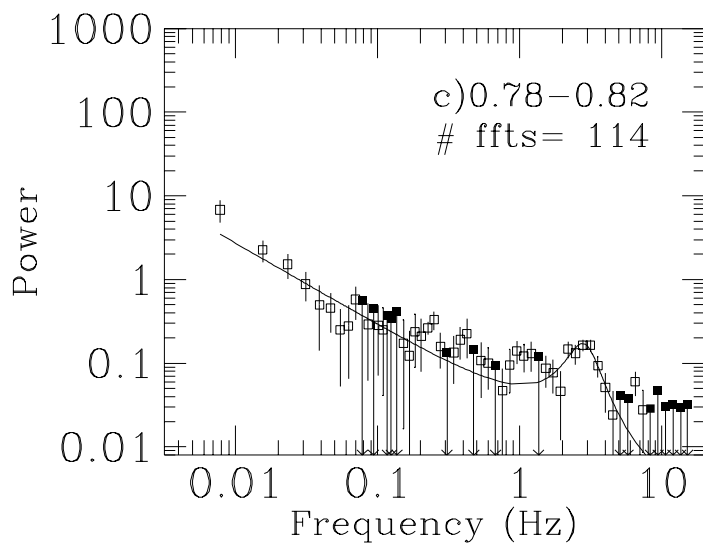
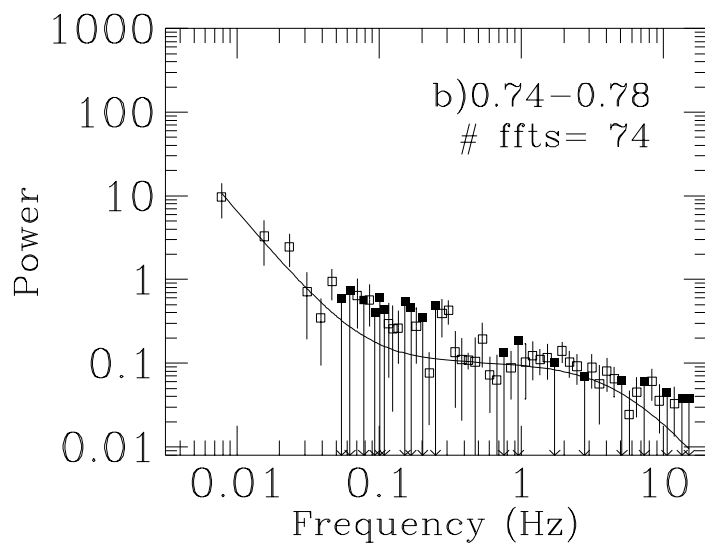
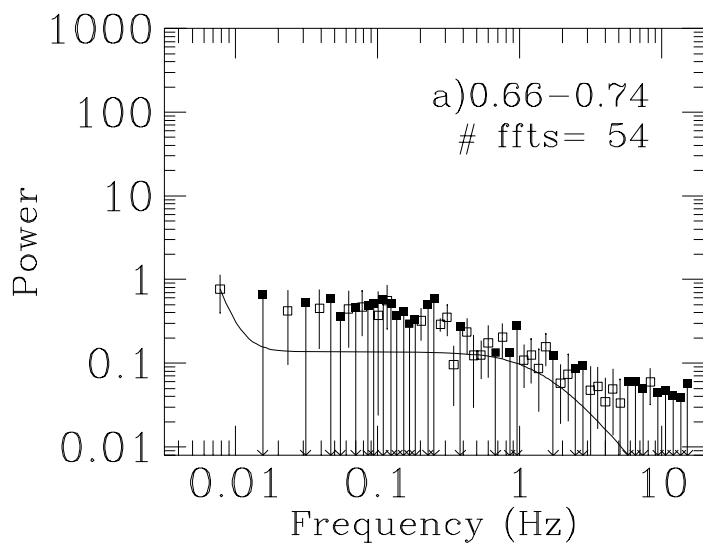


Figure 5

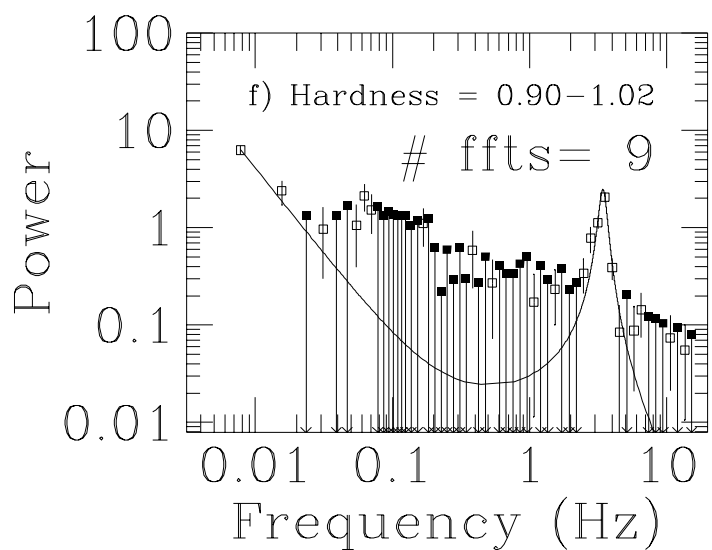
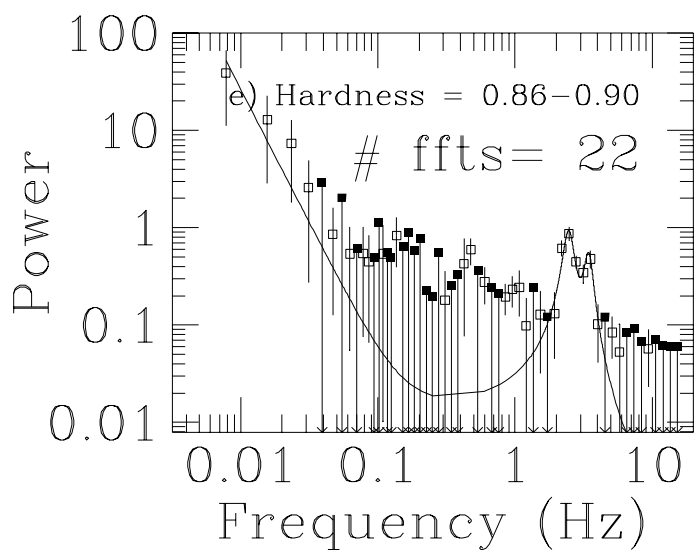
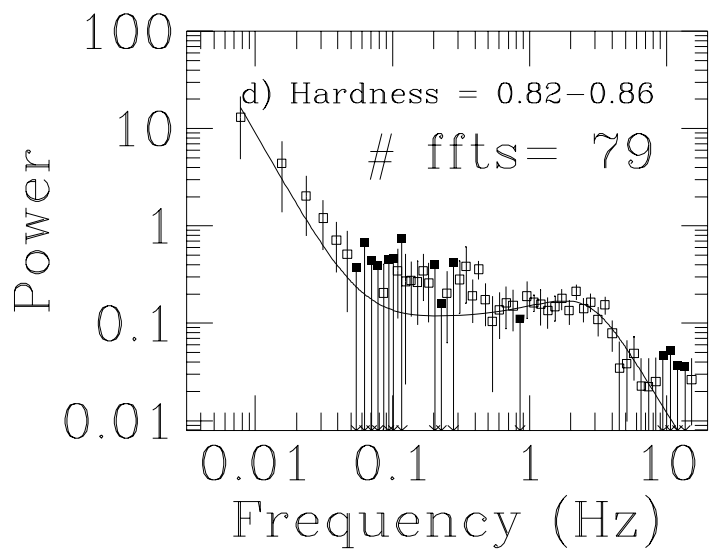
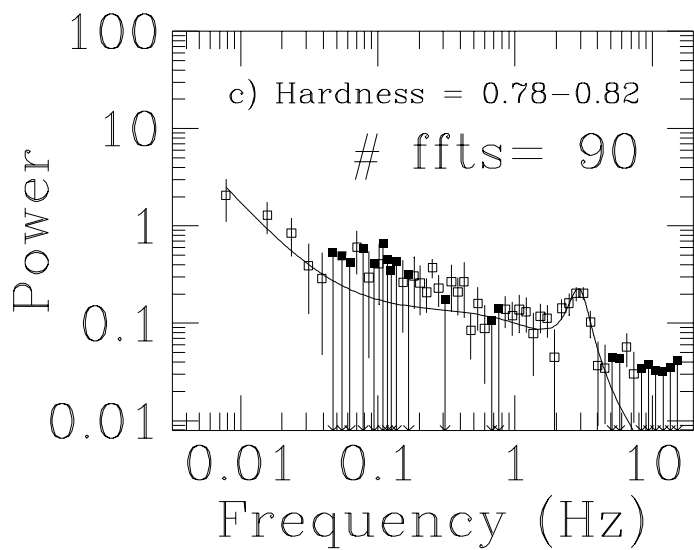
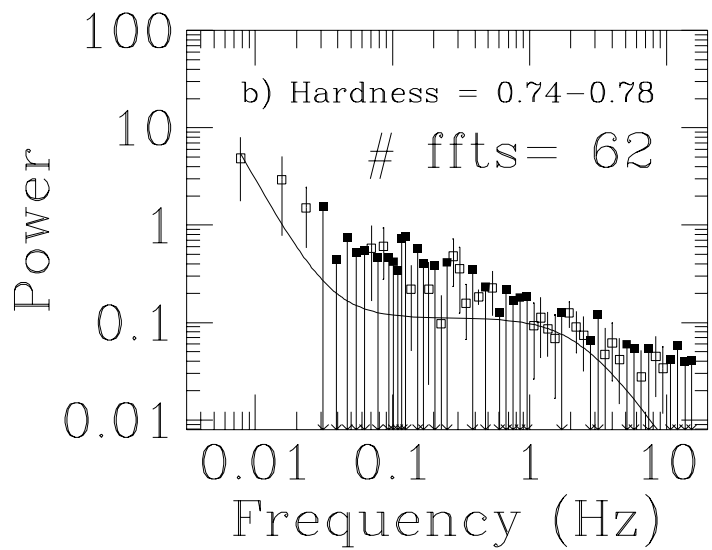
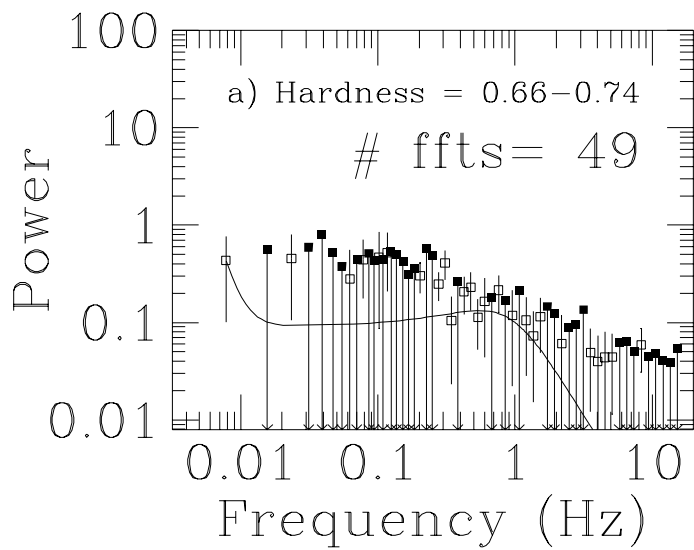


Figure 6

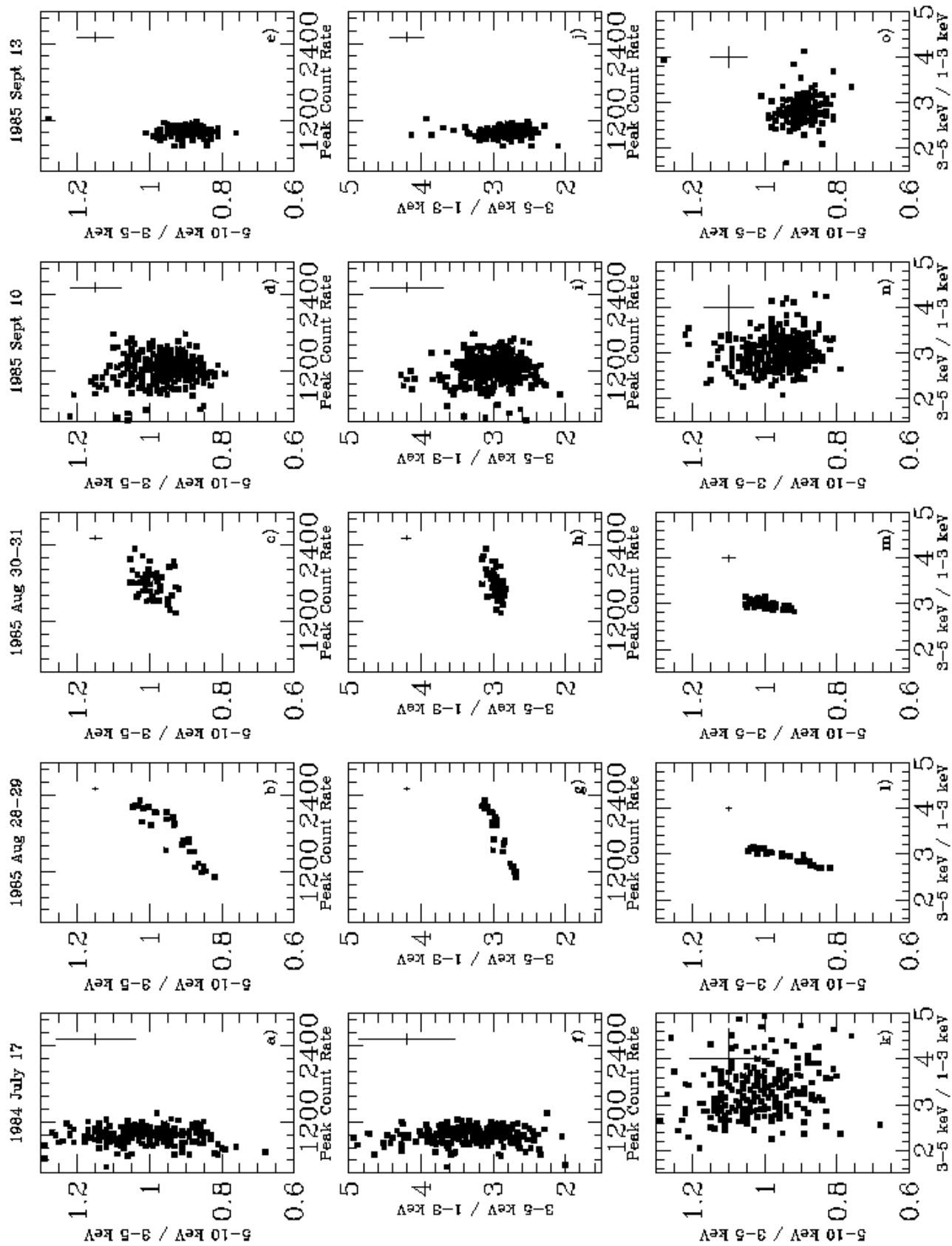


Figure 7

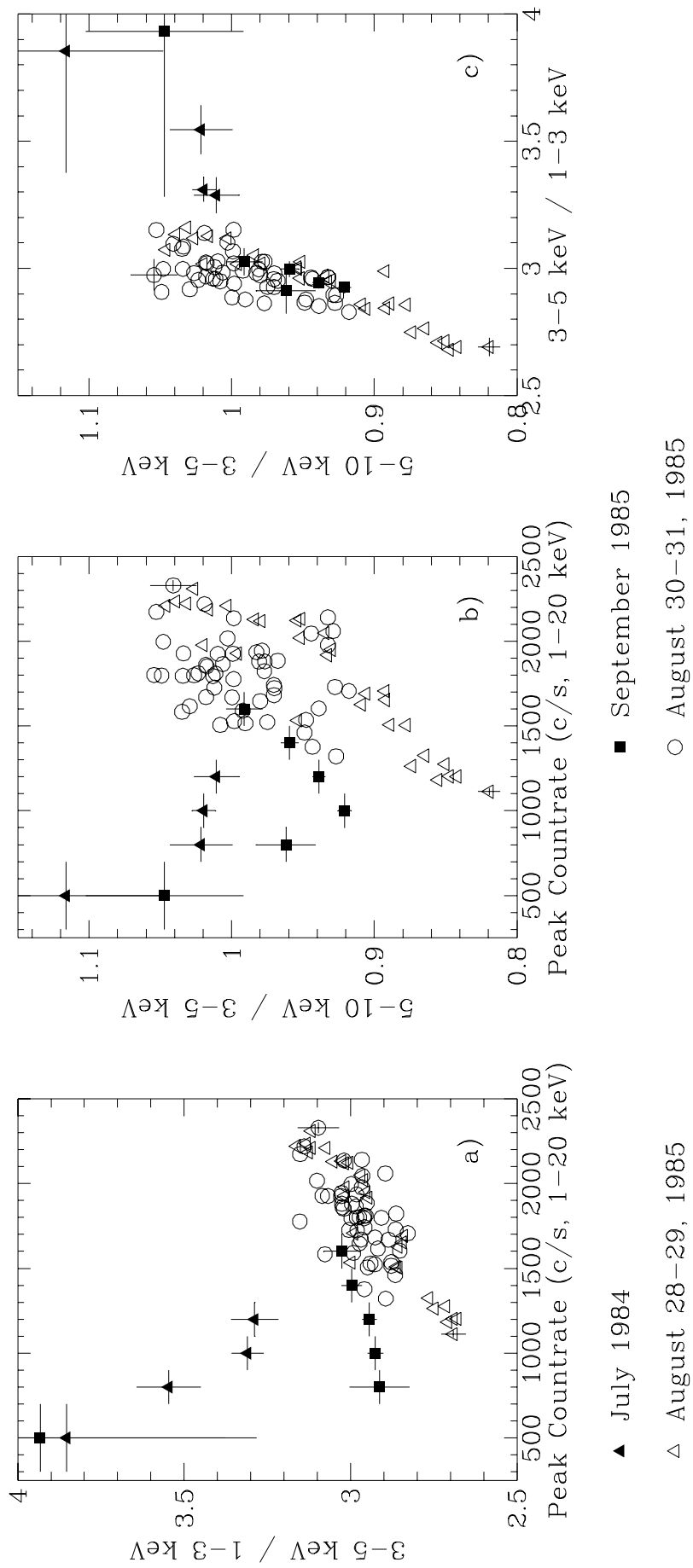


Figure 8

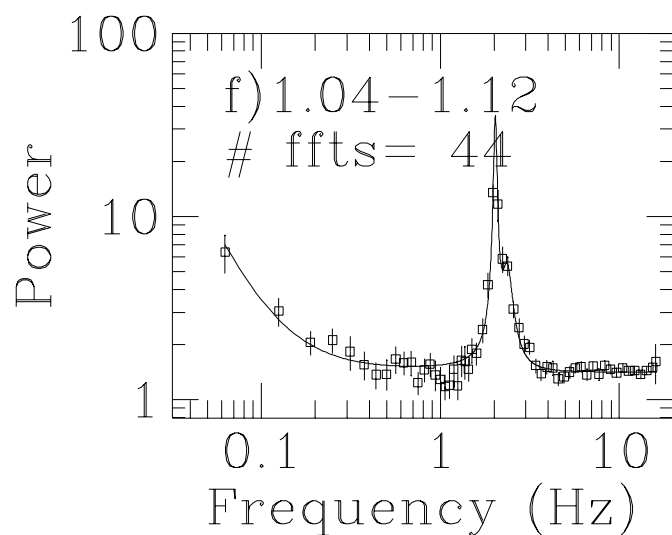
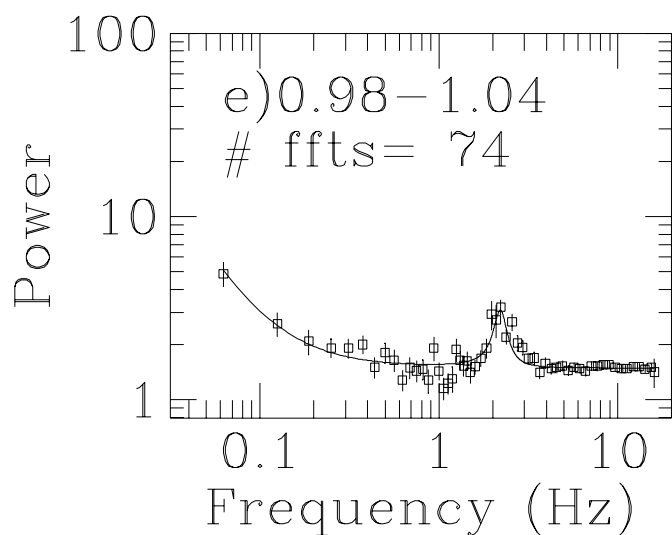
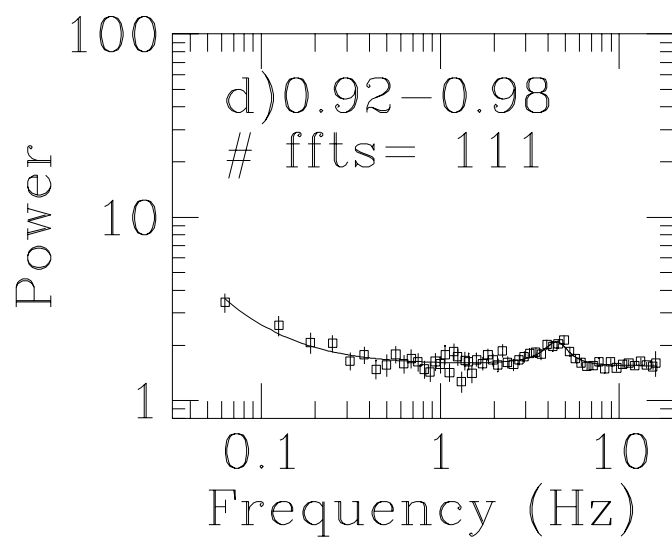
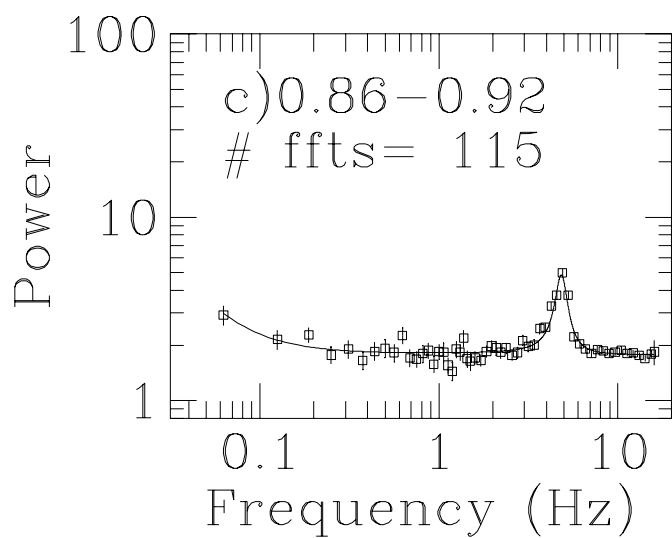
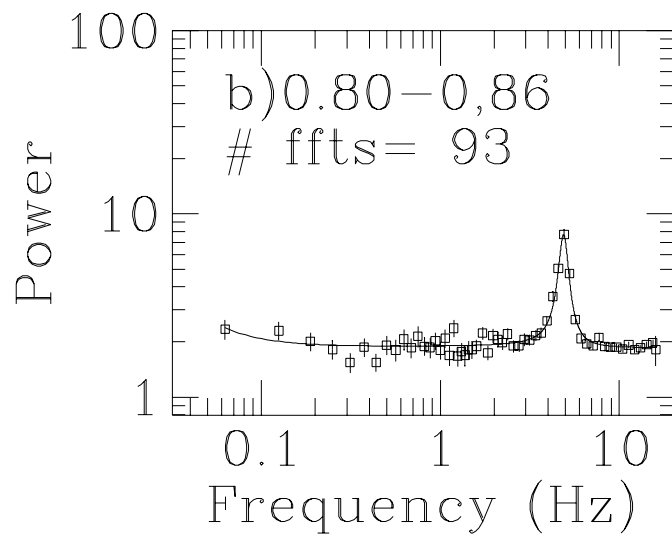
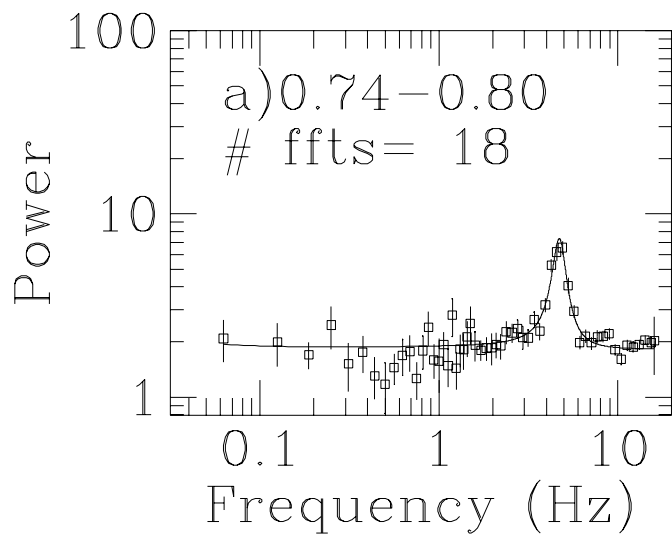


Figure 9

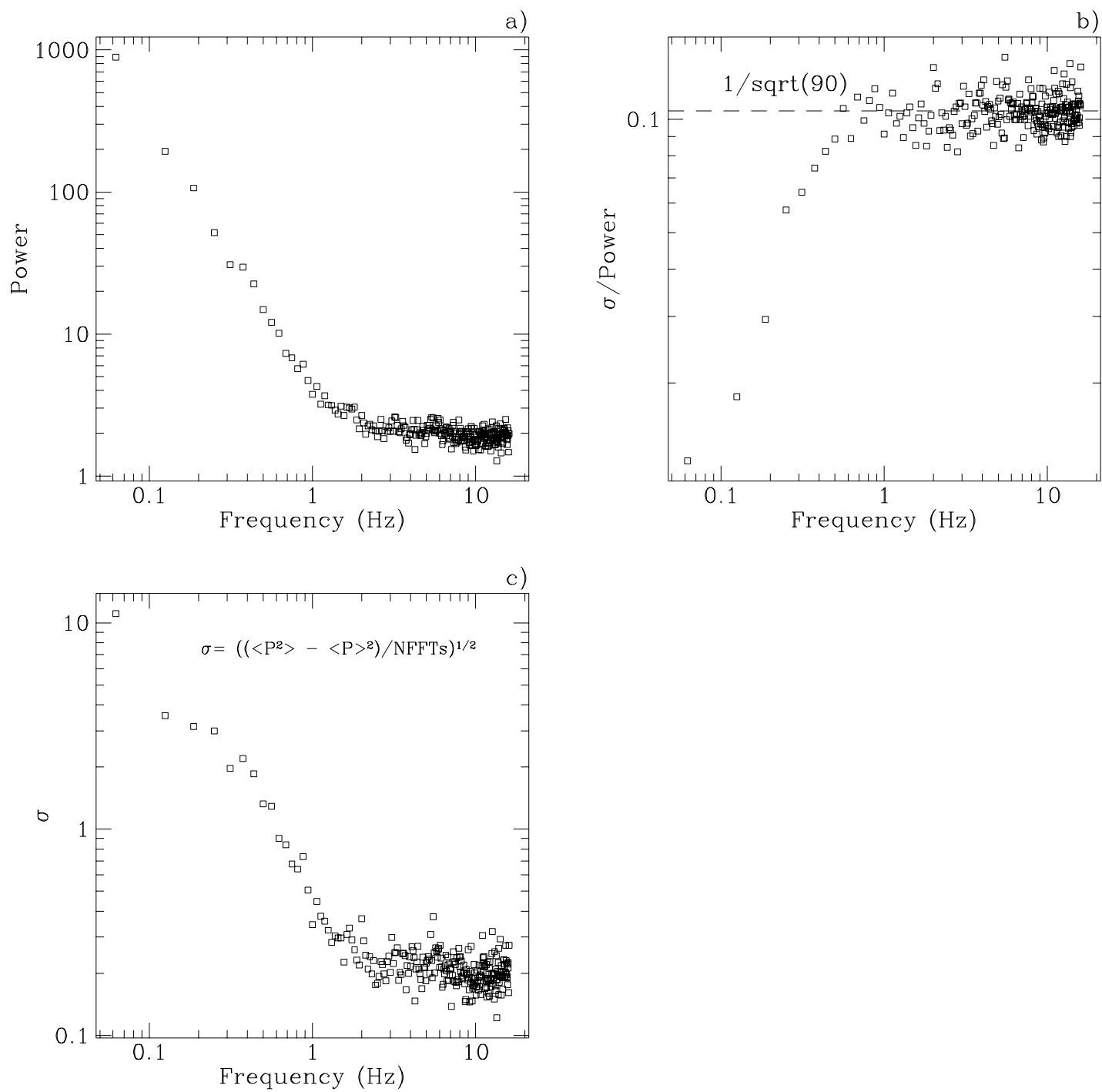
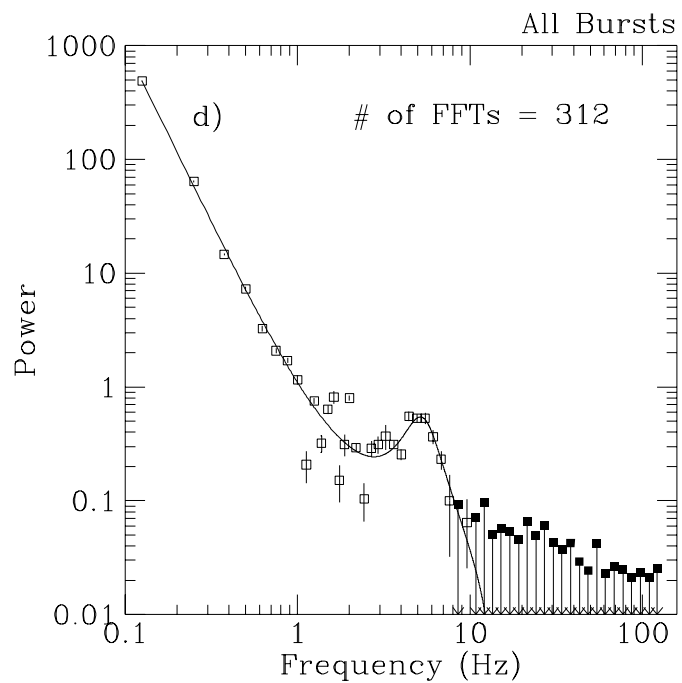
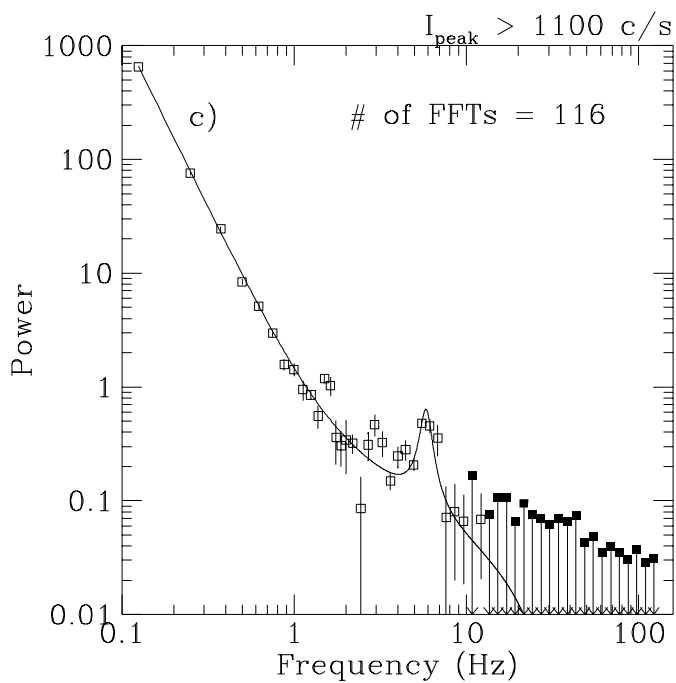
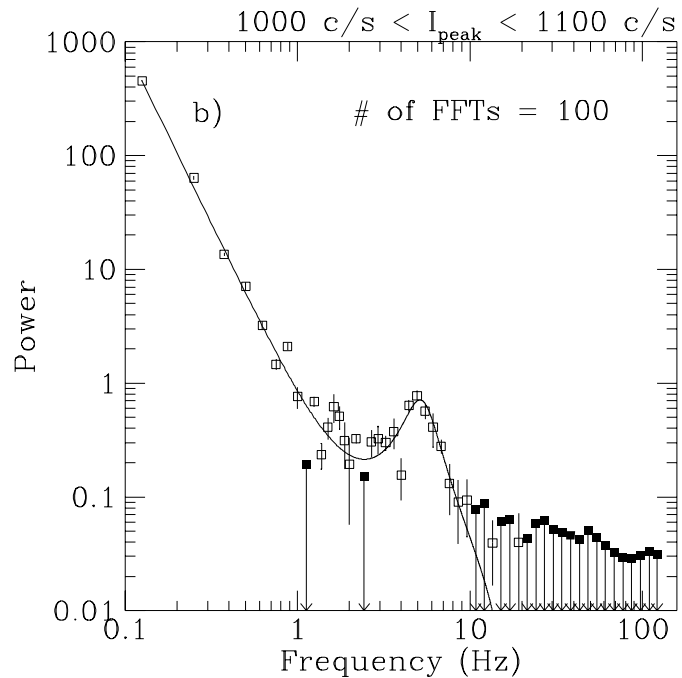
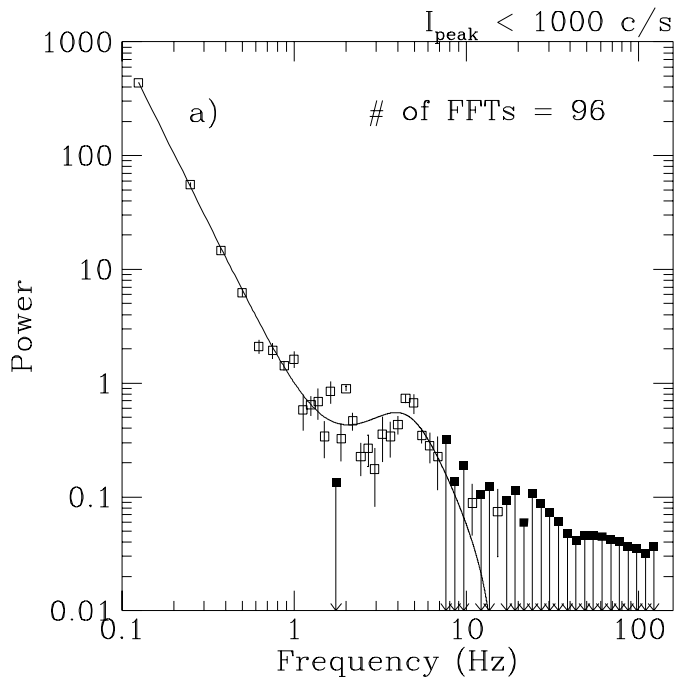


Figure 10



RB: Sept 10–13, 1985 (T3 data), Composite Fit

Figure 11

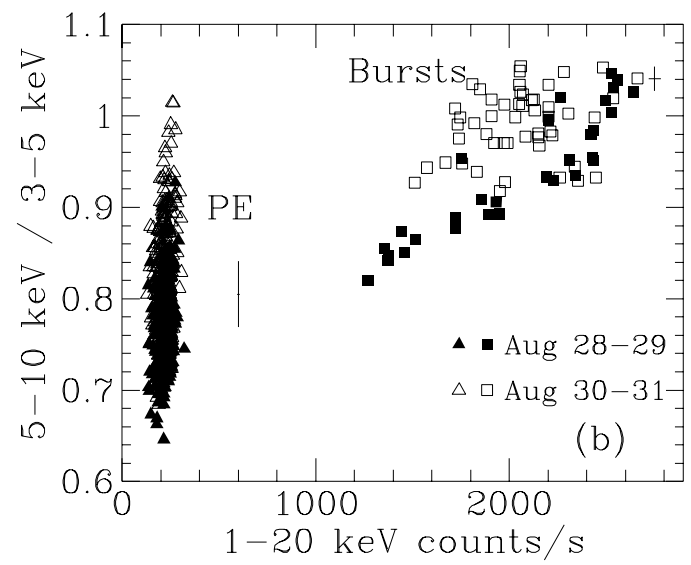
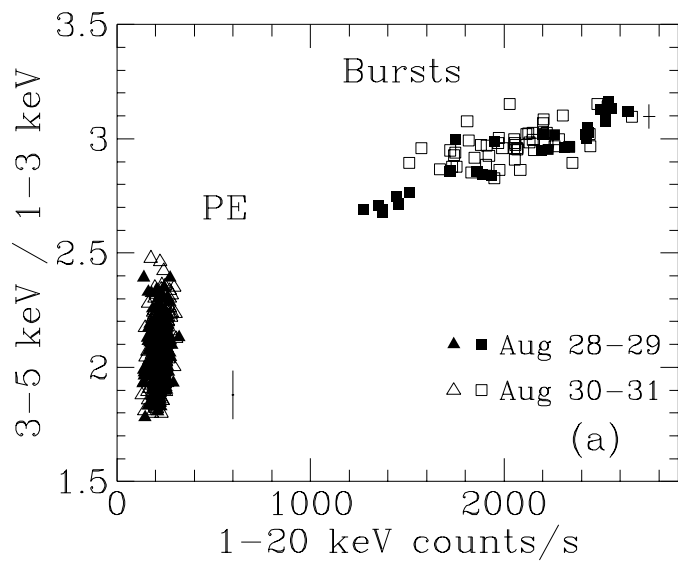


Figure 12

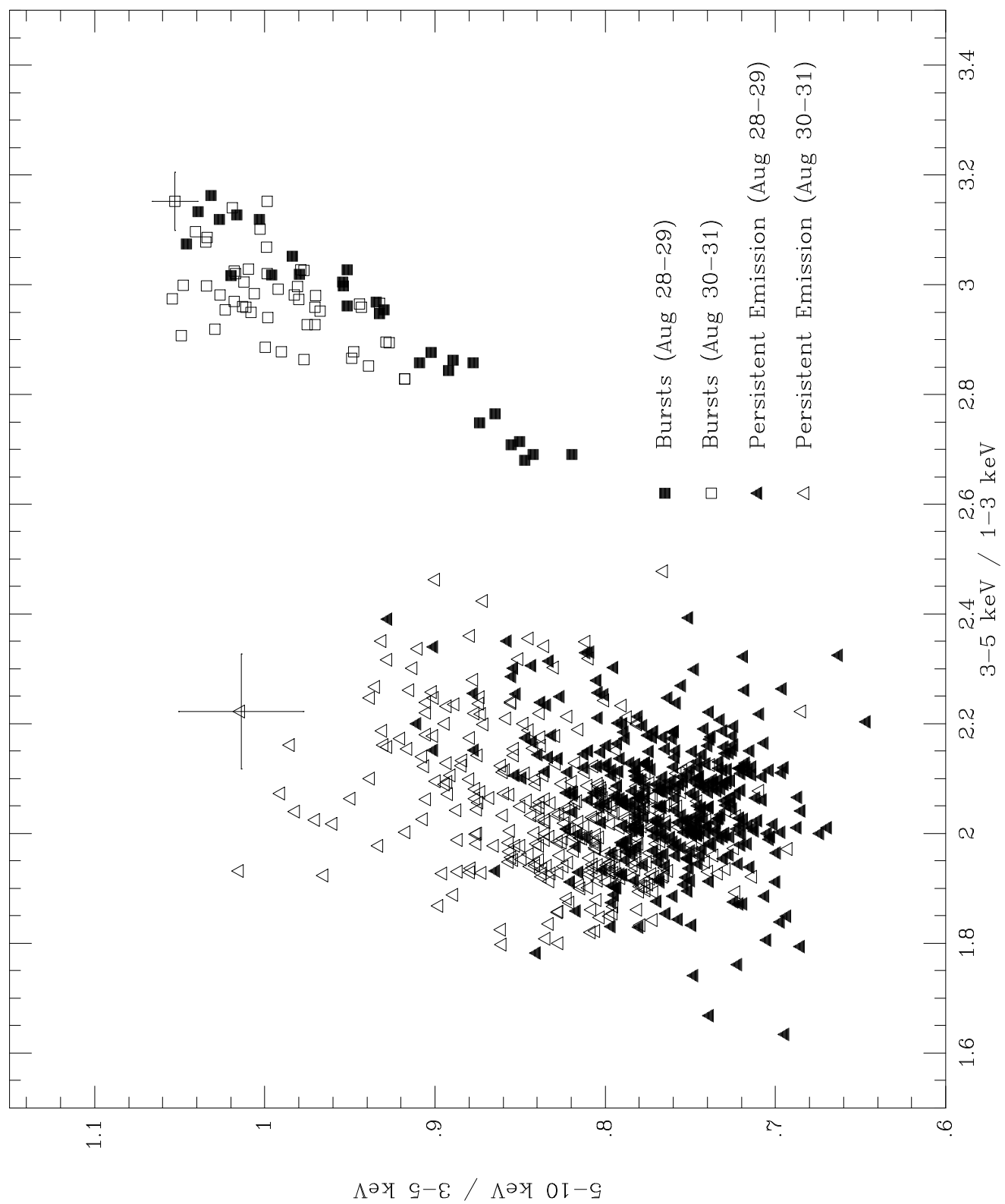


Figure 13

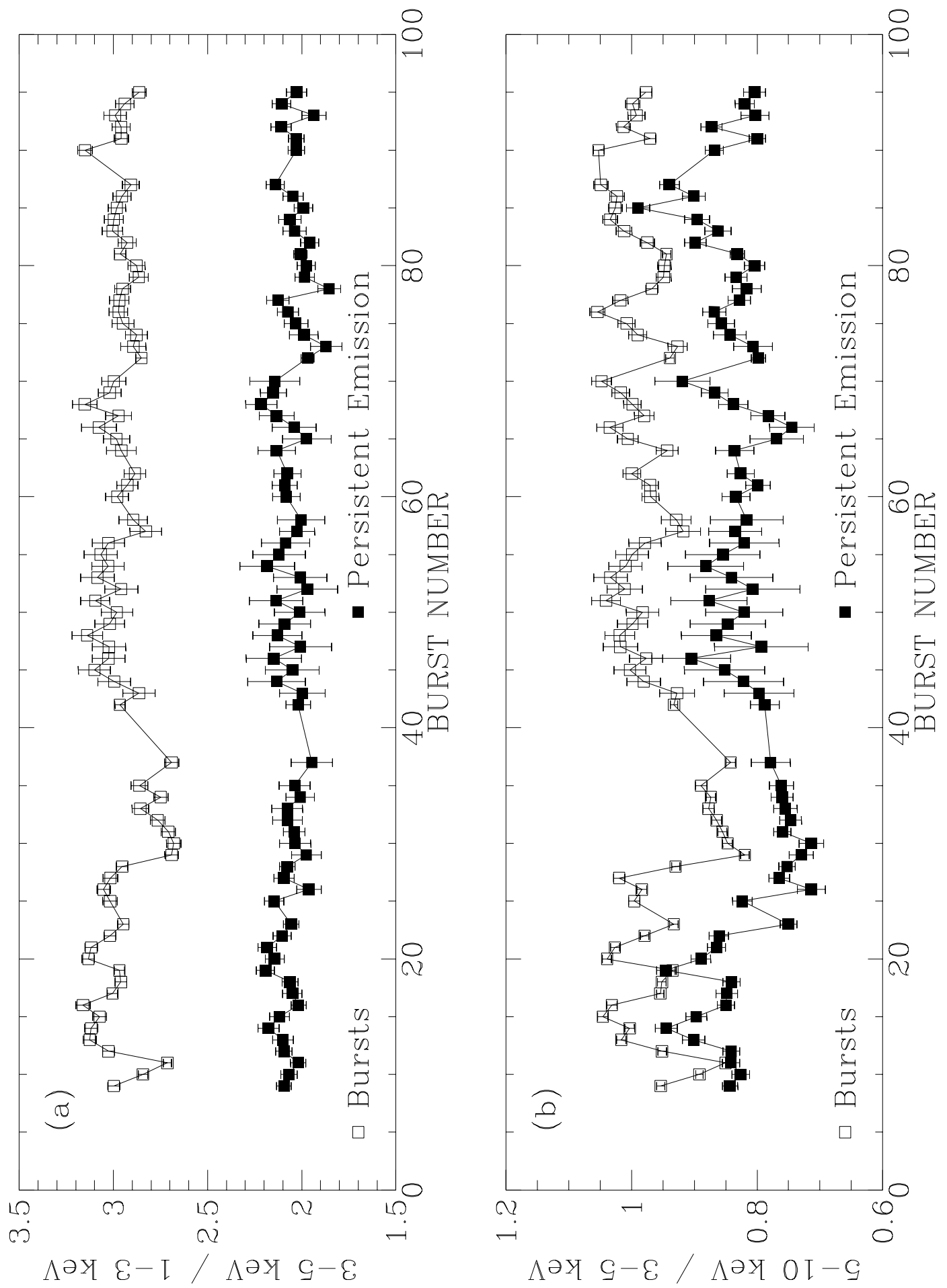


Figure 14

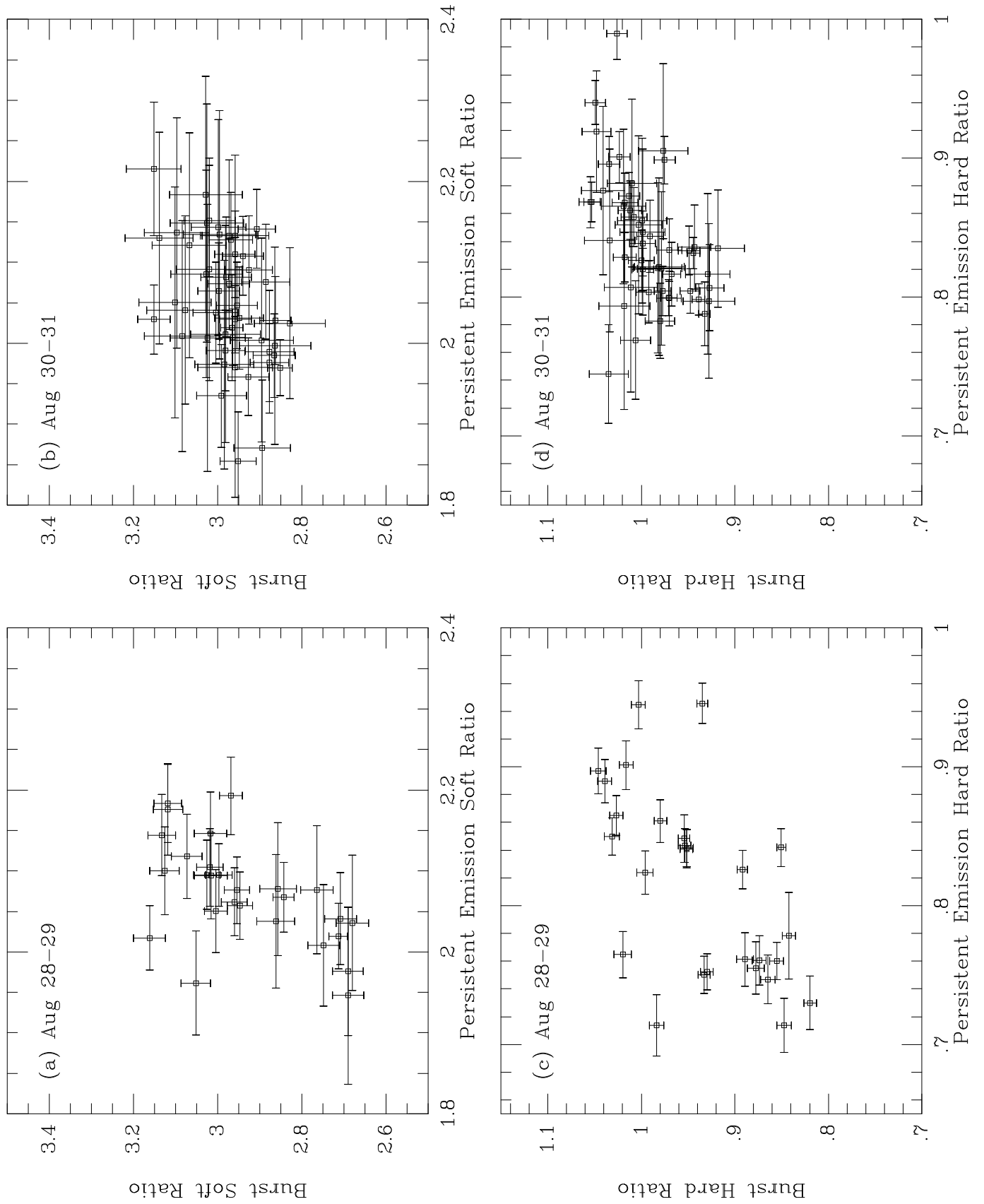


Figure 15

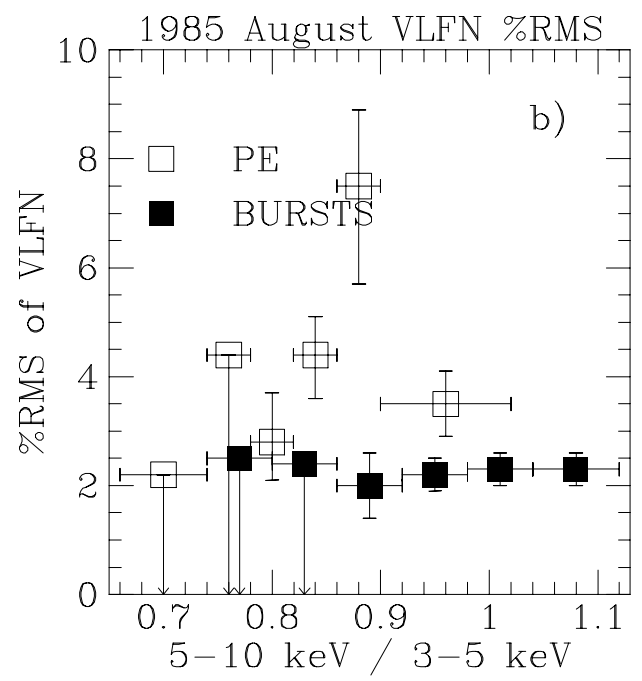
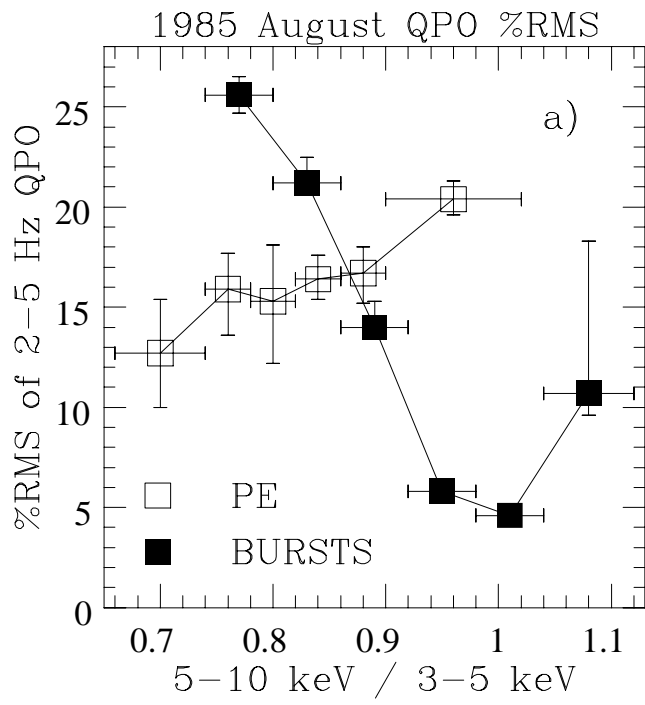


Figure 16

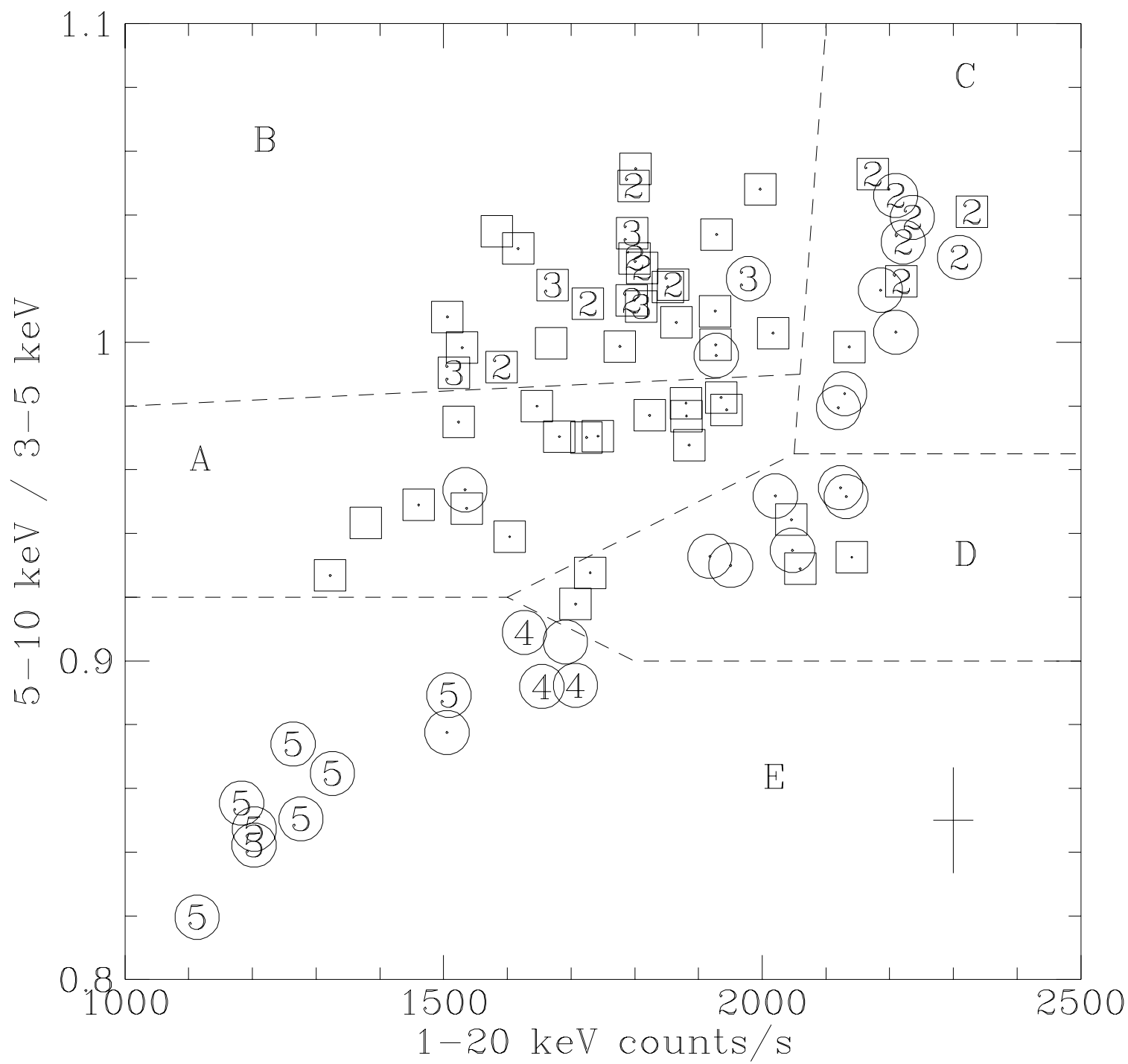


Figure 17

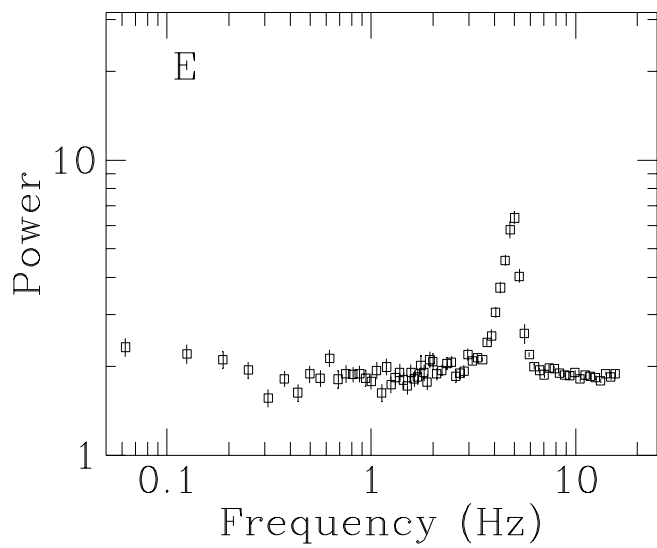
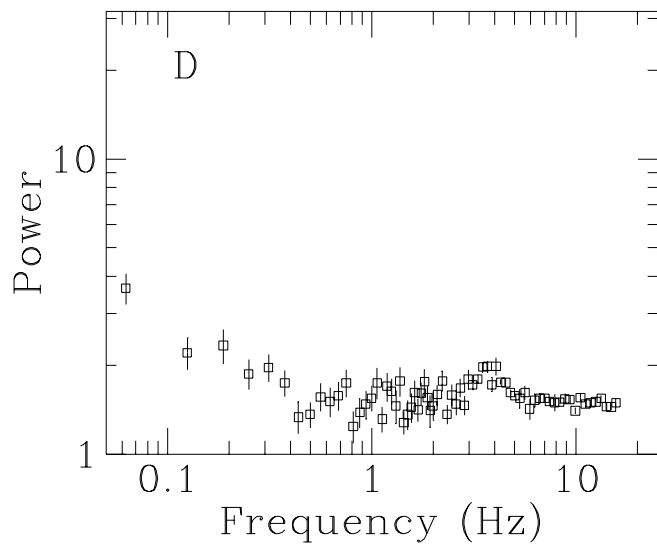
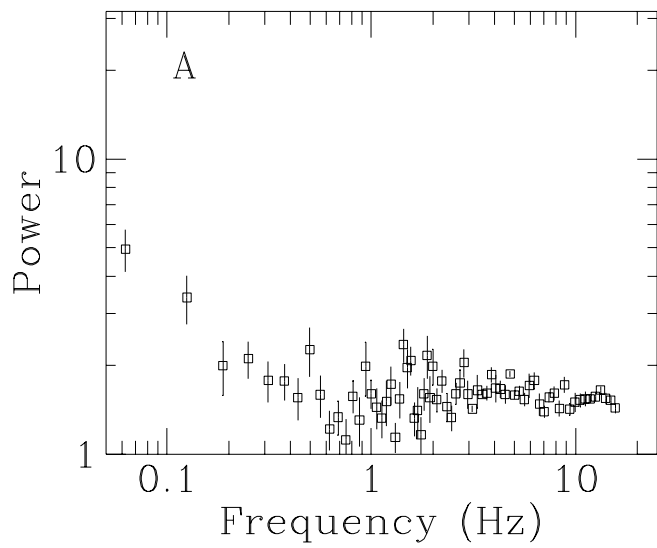
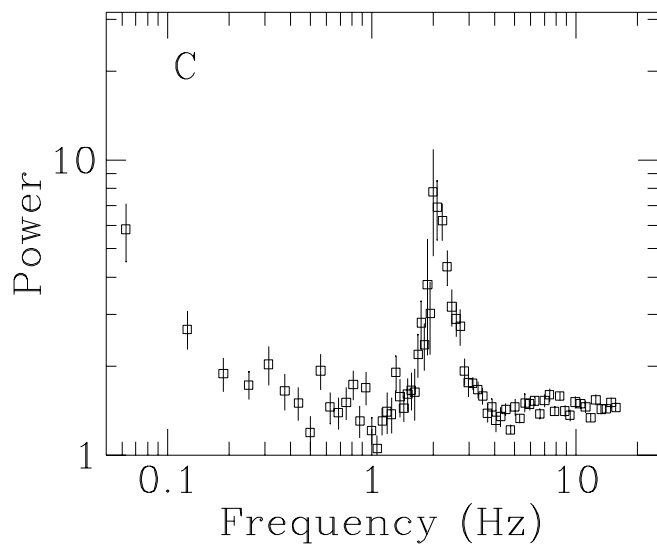
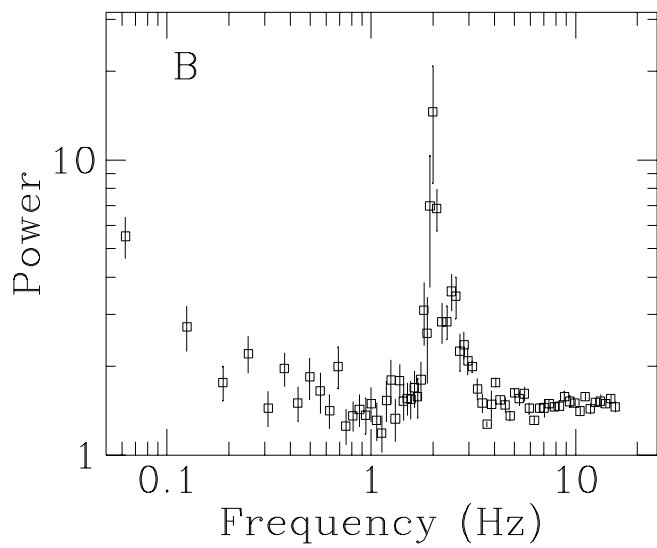
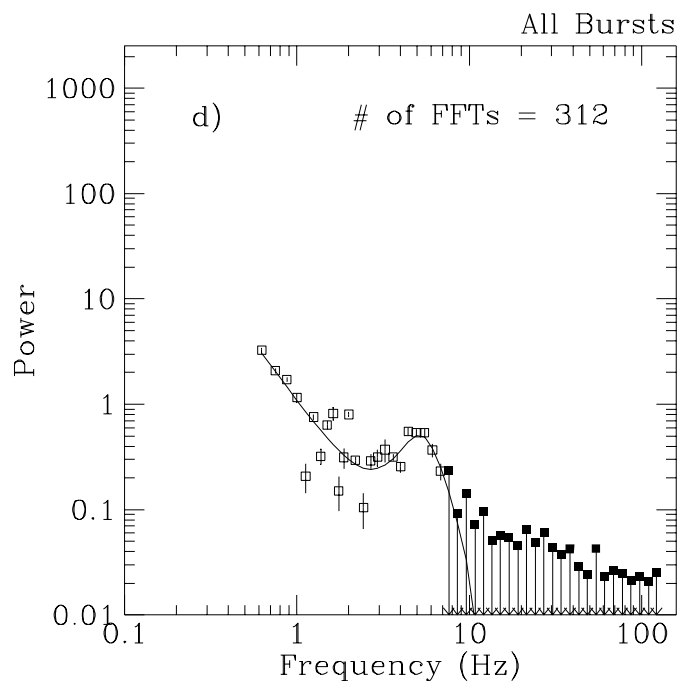
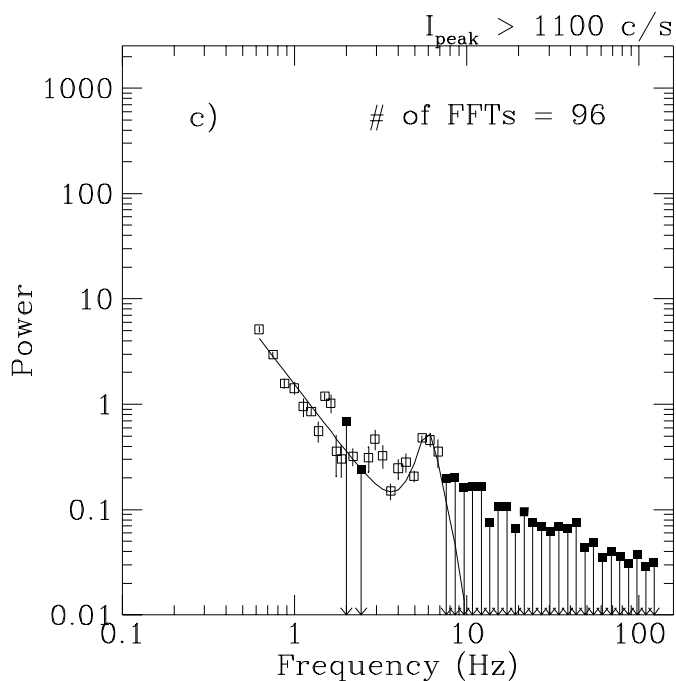
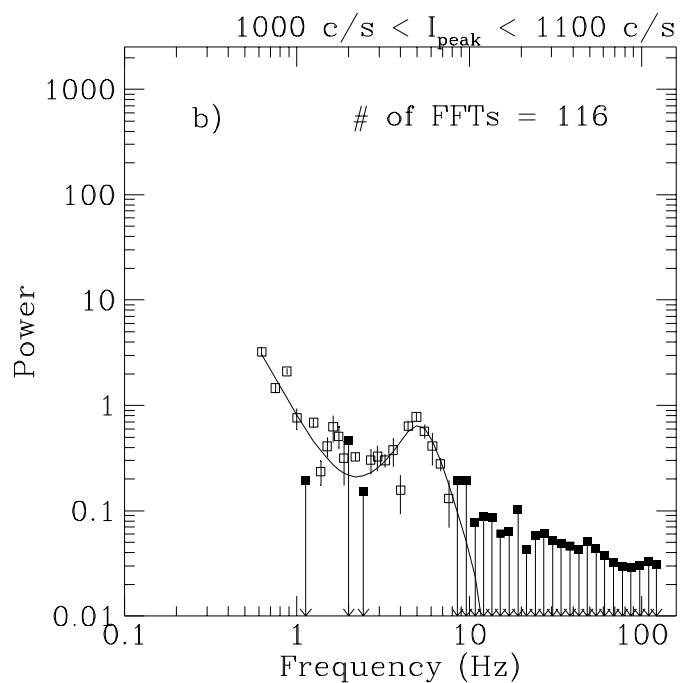
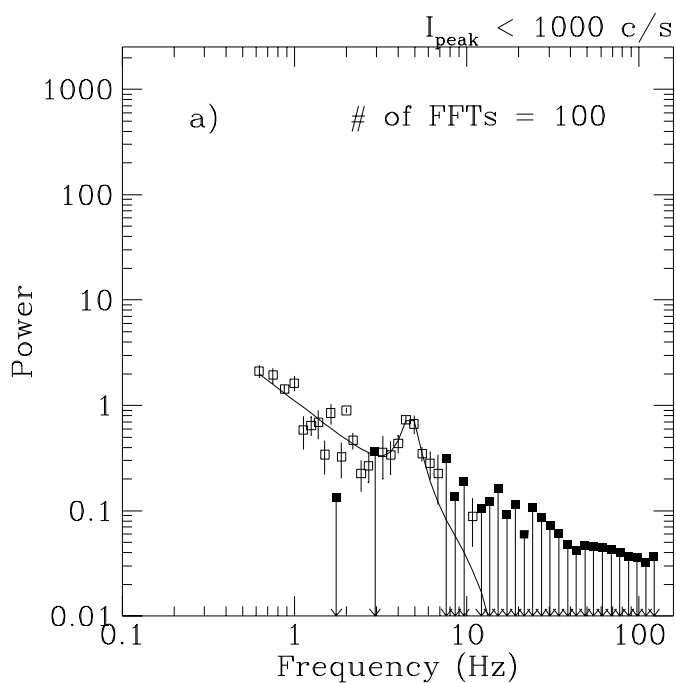
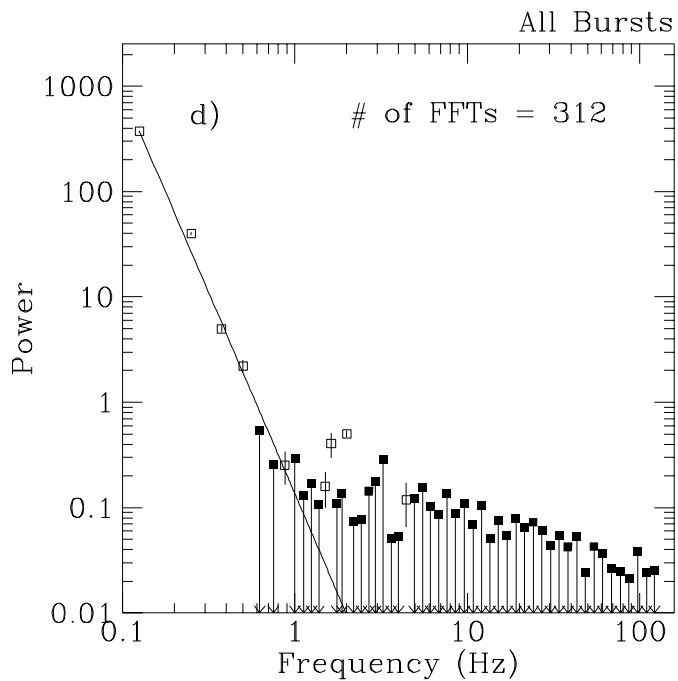
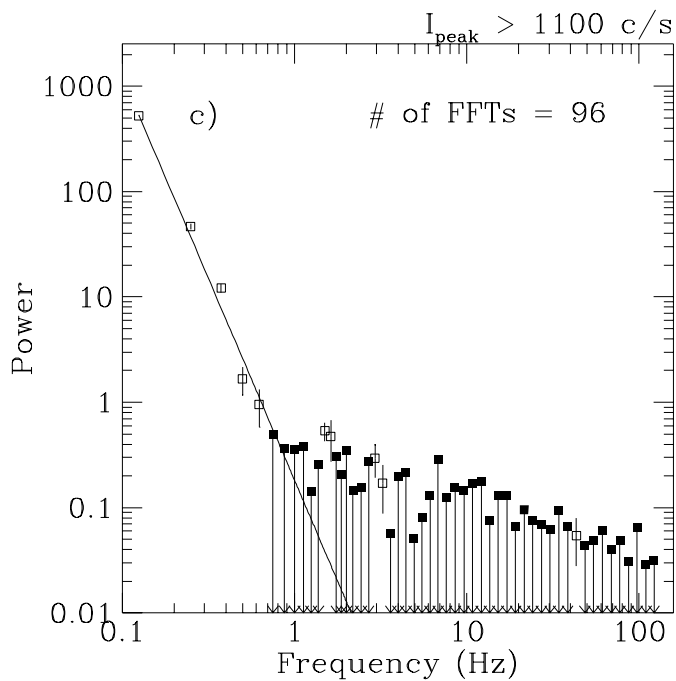
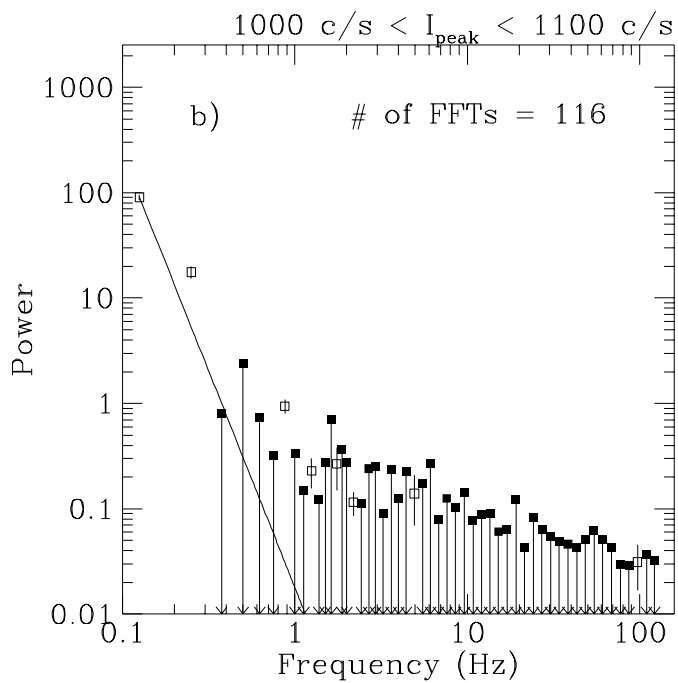
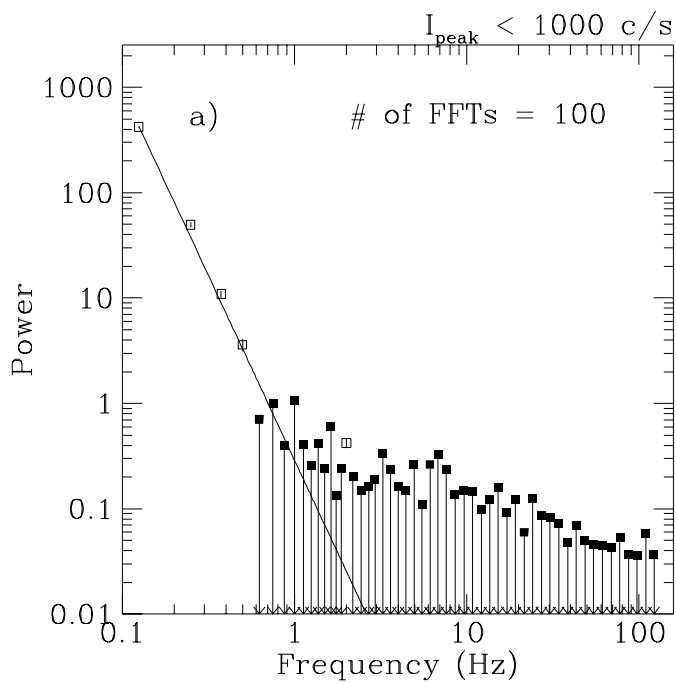


Figure 18



RB: Sept 10–13, 1985 (T3 data), Primary ($\nu > 0.6 \text{ Hz}$) Fits



RB: Sept 10–13, 1985 (T3 data), Residuals Fits